Heliyon 10 (2024) e24588

Contents lists available at ScienceDirect

Heliyon

journal homepage: www.cell.com/heliyon

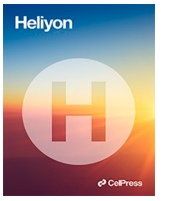

Research article

Synthesis, spectroscopic, chemical reactivity, topology analysis and molecular docking study of ethyl 5-hydroxy-2-thioxo-4-(p-tolyl)-6-(trifluoromethyl) hexahydropyrimidine-5-carboxylate

I. Umadevan [a], R. Rajasekaran [a,b], M. Anto Bennet [c], V. Rajmohan [d], V. Vetrivelan [e,**], K. Sankar [a], M. Raja [f,*]

[a] *Research and Development Centre, Bharathiar University, Coimbatore, 641046, Tamilnadu, India*
[b] *Department of Physics, Thiru Kolanjiappar Govt. Arts College, Virdhachalam, 606001, Tamilnadu, India*
[c] *Department of Electronics and Communications Engineering, Vel Tech Rangarajan Dr.Sagunthala R&D Institute of Science and Technology, Chennai, 600062, Tamilnadu, India*
[d] *Department of Electronics and Communications Engineering, Saveetha School of Engineering(SIMATS), Thandalam, Chennai, 602105, Tamilnadu, India*
[e] *Department of Physics, Government College of Engineering, Srirangam, Tiruchirappalli 620012, Tamilnadu, India*
[f] *Department of Physics, Govt. Thirumagal Mills College, Gudiyattam, 632602, Vellore, Tamilnadu, India*

A R T I C L E I N F O

Keywords:
PES
FT-IR
Topology
Electronic properties
Molecular docking

A B S T R A C T

The organofluorine hexahydropyrimidine derivatives are used in the drug discovery due to its steric nature to hydrogen and its extreme electronegativity. The Ethyl 5-hydroxy-2-thioxo-4-(*p*-tolyl)-6-(trifluoromethyl)hexahydropyrimidine-5-carboxylate (ETP5C) compound was synthesized and characterized by NMR (^{13}C and ^{1}H), FT-IR and UV–Vis spectroscopic techniques for experimentally and theoretically and elemental analyses, mass spectra also investigated. The most stable structure of synthesized molecule was studied by PES analysis in gas and liquid medium. The structural parameters such as bond length and bond angle of the title molecule have been obtained by DFT/B3LYP/6–311++G (d,p) set and compared with the structurally related experimental data of the compounds. The π-to-π* transition of the ETP5C molecule is identified using UV–Vis absorption spectral analysis. In addition, the chemical stability and reactivity are investigated using HOMO-LUMO analysis. The minimal HOMO-LUMO energy gap (4.6255 eV) clearly explains that the ETP5C molecule is more reactive for receptors. The nucleophilic and electrophilic regions such as active sites have been shown by MEP, ELF, LOL and Fukui functions. The second order optical effect has been explained by NLO analysis. The docking was performed with antineoplastic proteins that exhibit against the development of tumor cells.

* Corresponding author.
** Corresponding author.
E-mail addresses: vetri.tpgit@gmail.com (V. Vetrivelan), raja.physics2014@gmail.com (M. Raja).

https://doi.org/10.1016/j.heliyon.2024.e24588
Received 29 August 2023; Received in revised form 10 January 2024; Accepted 10 January 2024
Available online 17 January 2024

1. Introduction

Trifluoromethyl is an important functional group which possesses $–CF_3$ molecule by replacing hydrogen atoms in the methyl group by a fluorine atom. Trifluoromethylated derivatives are often used in pharmaceutical and fields. Many important pharmaceutical compounds incorporate trifluoromethyl functional group derivatives [1,2]. The organofluorine compounds lead one fourth place in the drug discovery due to its steric nature to hydrogen and its extreme electronegativity even though it has low molecular weight. So, fluorine atom has its biological applications in terms of protein binding affinity, lipophilicity, etc [3]. The organofluorine compounds exhibit biological properties such as protein-ligand binding, lipophilicity, etc due to its polarizability that is high. The fluorine atom influences the metabolic stability, membrane permeability of the substituents. So, organofluorine compounds can be used as anti-diabetic, *anti*-cholesterolemic, anti-emetic, anti-depressant, anti-inflammatory, anti-fungal and anti-bacterial drugs [4,5].

Nitrogenated heterocyclic compounds namely hexahydropyrimidine derivatives may be used to treat the fungi that responsible to dermatomycosis [6]. The pyrimidine derivatives can act as antimicrobial, anti-viral, anti-bacteria, anti-tubercular agents [7,8], anti-hypertensive, anti-tumor and membrane permeable agents [9] etc. Generally, Pyrimidine exists as heterocyclic aromatic organic molecule that contains 2 nitrogen atoms at six-member ring. Pyrimidine which is an integral portion of DNA or RNA gives applications in the biological and pharmacological field [10].

In addition, the above-mentioned compounds possess electronic and chemical properties and hence it can be used in industrial fields [1,9]. Meanwhile, the literature survey states that there had been no studies reported for the molecule 'Ethyl 5-hydroxy-2-thioxo-4-(*p*-tolyl)-6-(trifluoromethyl)hexahydropyrimidine-5-carboxylate' (ETP5C). So, the aromatic, heterocyclic, nitrogenated, organofluorine molecule ETP5C has been taken for the spectral and computational analyses in detail that may possesses some important biological, industrial and chemical activity.

In recent years, the study of theoretical modelling of cancer biomolecules with medical significance has benefited from the development of computer simulators, and it is now able to assess the important physical and chemical properties of approved biological compounds for cancer treatment using a range of theoretical methodologies. Density functional theory (DFT) has advanced with the establishment of a much more accurate exchange-correlation function and has developed into a magnificent tool in comparison to other traditional approaches because of its low processing cost and excellent accuracy [11–13].

The main objective of the present research work was to formulate, develop and optimize ETP5C calculated using DFT and compared with experimental data. To the best of my knowledge, no DFT investigations using topological analysis, PES, reactivity-based descriptor analyses and vibrational studies have ever been conducted on this title compound. In the present investigation, the focus of our study has been on figuring molecular geometry by connecting the desired attributes from an experimental assessment with the expected theoretical parameters of DFT.

The distribution of electrons and the reactive sites on the surface of the title compound were analysed using ESP (Electrostatic potential), ELF (Electron localization function) and LOL (Localized orbital locator). The charge transfer within the molecule was identified and frontier molecular orbitals (FMO) were plotted. The local reactivity descriptors like the local softness and Fukui function were obtained. Molecular docking studies were performed to identify the antiviral activity of the title compound on a couple of viral protein.

Studies utilizing both theoretical and experimental spectroscopic characterizations on Nuclear magnetic resonance (NMR), infrared and mass spectroscopy respectively. Using the molecular electrostatic potential map (MEP), Electron Localization Function (ELF), and Localized Orbital Locator (LOL), the distribution of electrons and reactive sites on the surface of the substance under investigation was examined. With the utilization of UV–Vis spectra, the electronic excited states of the title molecule were found and frontier molecular orbitals (FMO) analysis was used to investigate the intermolecular charge transfer within the molecule. The amount of distinct states that are accessible to electrons at a given energy level is known as the density of states, or DOS. The relative contribution of a given orbital or atom to the total DOS is indicated by the partial density of states (PDOS). The biological activity of title molecule is analysed for different antineoplastic proteins. We chose them for the current studies based on the literature review since the title chemical ETP5C has not been previously investigated with these specific antineoplastic proteins.

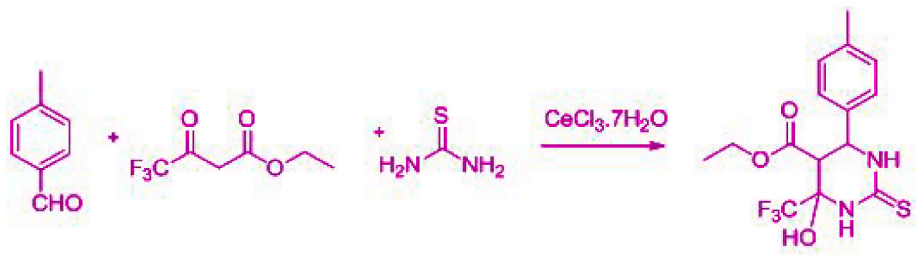

Fig. 1. Schematic representation of the synthesis of ETP5C.

2. Material and methods

2.1. Synthesis of ETP5C

We mixed 1.2 mL of *p*-tolualdehyde (0.01 mol), 2.3 g of thiourea (0.03 mol), 1.5 mL of ethyl 4,4,4-trifluoroacetoacetate (0.01 mol) and 25 % of cerium chloride heptahydrate in 40 mL of ethanol in a flask. An inert environment at 80 °C was used to stir the reaction mixture for 12 h. An ice-cold water solution was added to the reaction mixture after the cooled mixture had been poured into the cooled solution after thin-layer chromatography confirmed the reaction had completed. A suction filter was used to separate the solids and ice-cold water was used to wash them. After recrystallizing from ethanol, the crude product becomes pure. In Fig. 1, we can see the reaction.

2.2. Experimental methods

The FT-IR spectrum has been recorded in the region 4000-400 cm^{-1} by KBr pellet technique with 1–10 cm^{-1} resolution on a perkin elmer FT-IR spectrometer. The nuclear magnetic analysis namely ^{13}C and $^{1}HNMR$ spectra was recorded using the DMSO solvent by Bruker Avance III 500 MHz high-resolution NMR spectrometer. The UV–Vis absorption spectrum of ETP5C was examined using the DMSO solvent in the range 200–600 nm by PerkinElmer LAMBDA 950 UV spectrometer instrument. Mass spectra recorded by high resolution mass spectrometer (LC-QTOF-HRMS). The above-mentioned spectral studies were taken at SAIF, IIT-Madras, India.

2.3. Computational details

The software Gaussian 09W was used with the method of DFT/B3LYP/basis set of 6–311++G (d,p) [14–16] for the analysis of the properties of ETP5C molecule. The potential energy scan analyses were performed for title molecule using gas phase and DMSO solution phase. The vibrational assignments have been performed by Potential Energy Distribution (PED) calculations. The Potential Energy Distribution (PED) calculation has also performed by taking VEDA output which helps to know the type of vibrations and functional group [17]. The FT-IR vibrational frequencies were calculated and scaled using 0.961scaling factor to compare with experimental values. The proton NMR (^{1}H) chemical shift values obtained by GIAO approach are correlated with the experimental values [18]. TD-DFT method with Gaussian 09W program has been used for UV–Vis analysis. Multiwfn software has been used to visualize the molecule in terms of Topology to know the electronic and chemical properties [19]. The mapped MEP surfaces and HOMO-LUMO are graphed with the GaussView program [20]. The individual atomic reactivity sites have been performed by Mulliken charges and Fukui functions analysis [21]. The atomic interaction energy between ligand ETP5C with the selected proteins is identified by 1.4.6 version of Auto-dock and Pymol software [22] to know the biological activity.

3. Results and discussion

3.1. PES conformational analyses

The stability of the ETP5C molecule is analysed using gas phase and DMSO solvent phase. The present study, the minimum energy conformer is in order to identify for two dihedral (SC1: C24–C23–O22–C20 and SC2: C23–O22–C20–C2) angles. The dihedral angle is rotated 0–360° is split 10 steps and each step size is 36°. The 2 dimensional PES (Gas and DMSO) coordinates are represented of title

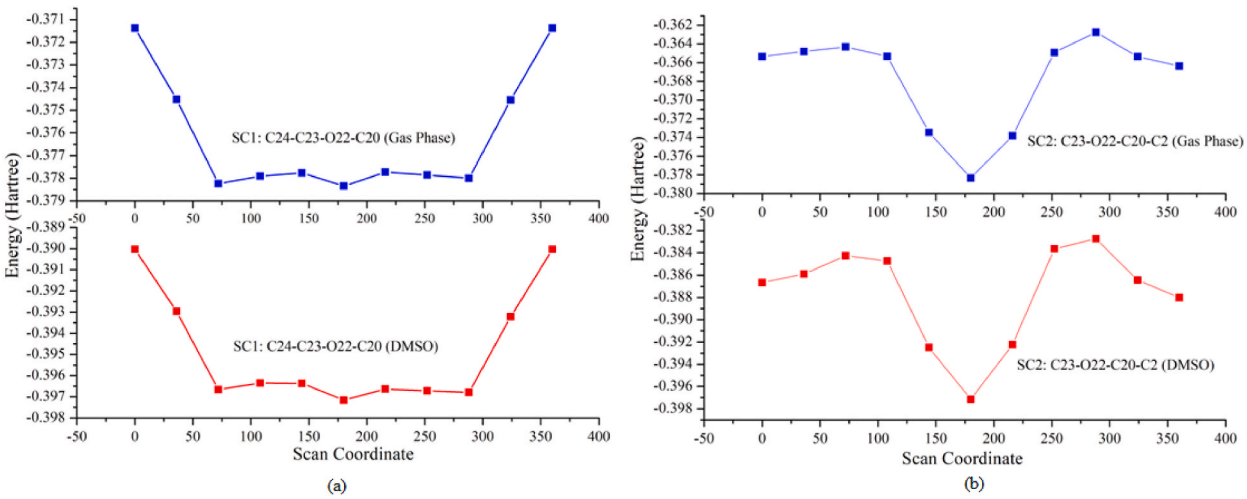

Fig. 2. 2D-Potential energy surface scan: (a) SC1: C24–C23–O22–C20, (b) SC2: C23–O22–C20–C2 of title molecule.

molecule as show in Fig. 2a-b. The minimum energy of title molecule is observed at gas phase: energy (E) = −0.3783 hartree, dihedral angle is SC1 -180.004, SC2 – 180.003° and DMSO solvent observed at energy (E) = −0.3971 hartree, dihedral angle is SC1 -180.004 and SC2 – 180.003°.

3.2. Molecular geometry

The minimum energy conformers of title molecule is optimized for gas phase and DMSO solvent phase using DFT/B3LYP/6–311++G (d,p) basis set. The optimized structure of ETP5C has been shown in Fig. 3. The structural parameters such as bond length, bond angle and RMSD values have been shown in Table 1. There is no XRD data for the title molecule and hence structurally related XRD data has been collected to compare the theoretical data of the title molecule through literature survey [23,24]. The theoretical structural parameter data are accordance to reference experimental value.

The theoretical C–C bond length of the title molecule has been observed between 1.532–1.382 Å(gas phase), 1.574 to 1.392 Å (DMSO), while C–H bond length observed at 1.090 to 1.080 Å (gas phase), 1.091 to 1.084 Å (DMSO). Generally, bond length decides the strength of the bonds by employing inverted nature between length and strength. Furthermore, the bond is so strong when electron participation is high and hence the length small. So, the C–H bonds of the title molecule are stronger than the C–C bonds. The RMSD values are calculated for gas Phase and DMSO solvent of title molecule. The RMSD values of bond length observed at 0.0739 Å (gas Phase), 0.0784 (DMSO) and bond angles are observed at 0.6164 (gas Phase) and 1.5570° (DMSO). The bond lengths for C–N, C–F, F–H, O–C and C–S atoms have also been reported in Table 1 with the bond angle.

3.3. Nuclear magnetic analysis

The structural, chemical and magnetic behaviour of synthesized molecule can be characterized by NMR with help of chemical shifts. The chemical shift of carbon and hydrogen atoms arrives by the resonance frequency between the molecule and the external magnetic field. The resulting chemical shifts appear in the form of distortion or in the form of wide resonance peaks for carbon and protons are taken into account. Molecular shifts are so accurate if the molecule is small [19,25]. The B3LYP/GIAO/6–311++G (d,p) with DMSO solvent method utilized to compute the chemical shift values of ETP5C. This method is so accurate while comparing with other methods. The C_{13} and ^{1}H NMR of ETP5C has been obtained experimentally and shown in Figs. 4 and 5 to understand the chemical environment of ETP5C. The experimental and theoretical chemical shifts of ETP5C were reported in Tables 2 and 3. The experimental C_{13} chemical shifts of title molecule is observed between from 190.04 to 21.58 ppm and theoretically observed between from 189.91 to 22.46 ppm.

The maximum chemical shift is observed C5 (exp-190.04 ppm, theo-189.91 ppm), C20 (exp-167.43 ppm, theo-168.23 ppm) and C8 (exp157.35 ppm, theo-157.55 ppm) atoms because the halogen atoms and highly electronegative atoms are bonded. The sulphur atom is bonded for C5 (S12–C5) atom, the two oxygen atoms are attached with C20 (C20–O21, C20–O22) atom and three fluorine atoms are attached with C8 (F9–C8, F10–C8 and F11–C8) atom. The lowest chemical shift of C13 NMR is observed C19 (exp-46.74 ppm, theo-

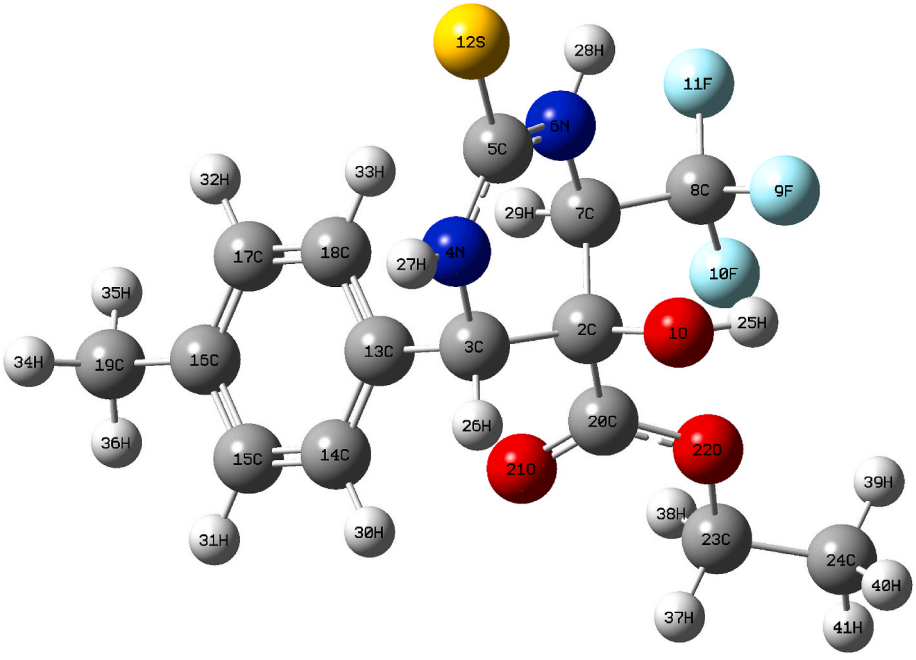

Fig. 3. Optimized geometrical structure of ETP5C by B3LYP/6–311++G (d,p) basis set.

Table 1
Optimized geometrical bond length (Å) and bond angle (°) of ETP5C: Theoretical and experimental (a*) bond lengths and bond angles.

Parameters	Bond length(°)			Parameters	Bond angle(°)		
	Gas Phase	DMSO	Experimental (a*)		Gas Phase	DMSO	Experimental (a*)
(O1–C2)	1.429	1.411	1.422	(C2–O1–H25)	114.0	110.9	
(O1–H25)	0.967	0.964		(O1–C2–C3)	109.6	108.6	110.24
(C2–C3)	1.532	1.574	1.497	(O1–C2–C7)	109.6	112.5	110.24
(C2–C7)	1.532	1.555	1.497	(O1–C2–C20)	109.6	112.4	110.24
(C2–C20)	1.507	1.559	1.462	(O1–H25–F9)	119.5	140.0	
(C3–N4)	1.464	1.463	1.413	(C3–C2–C7)	108.6	107.6	109.20
(C3–C13)	1.507	1.521	1.492	(C3–C2–C20)	109.6	108.6	109.20
(C3–H26)	1.090	1.091	0.970	(C2–C3–C4)	109.2	107.1	
(N4–C5)	1.341	1.338	1.339	(C2–C3–C13)	109.5	110.8	109.50
(N4–H27)	0.970	1.009		(C2–C3–H26)	109.5	107.5	109.30
(C5–N6)	1.341	1.353	1.339	(C7–C2–C20)	109.8	108.7	
(C5–S12)	1.712	1.706		(C2–C7–N6)	109.2	109.7	109.20
(N6–C7)	1.464	1.455	1.462	(C2–C7–C8)	109.6	114.7	109.50
(N6–H28)	0.970	1.009		(C2–C7–H29)	109.5	107.4	109.50
(C7–C8)	1.530	1.536	1.497	(C2–C20–N21)	120.0	118.5	
(C7–H29)	1.090	1.093	0.970	(C2–C20–N22)	120.0	122.8	121.70
(C8–F9)	1.399	1.360		(N4–C3–C13)	109.5	110.3	109.20
(C8–F10)	1.399	1.338		(N4–C3–H26)	109.5	106.3	
(C8–F11)	1.399	1.346		(C3–N4–C5)	121.3	125.9	
(C13–C14)	1.382	1.397	1.385	(C3–N4–H27)	119.3	117.8	
(C13–C18)	1.382	1.398	1.385	(C13–C3–H26)	109.6	108.1	
(C14–C15)	1.382	1.392	1.385	(C3–C13–C14)	120.0	119.3	
(C14–H30)	1.080	1.085	0.970	(C3–C13–C18)	120.0	120.3	119.20
(C15–C16)	1.382	1.399	1.385	(C5–N4–H27)	119.3	116.2	118.50
(C15–H31)	1.080	1.085	0.980	(N4–C5–N6)	122.6	119.2	121.40
(C16–C17)	1.382	1.399	1.390	(N4–C5–S12)	118.7	122.0	
(C16–C19)	1.507	1.509	1.497	(N6–C5–S12)	118.7	120.8	
(C17–C18)	1.382	1.392	1.385	(C5–N6–C7)	121.3	122.7	121.40
(C17–H32)	1.080	1.085	0.970	(C5–N6–H28)	119.3	115.6	
(C18–H33)	1.081	1.084	0.980	(C7–N6–H28)	119.3	118.4	
(C19–H34)	1.090	1.095	0.980	(N6–C7–C8)	109.5	107.5	
(C19–H35)	1.090	1.092	0.980	(N6–C7–H29)	109.5	112.0	
(C19–H36)	1.090	1.092	0.980	(C8–C7–H29)	109.6	105.5	109.30
(C20–N21)	1.208	1.209		(C7–C8–F9)	109.5	112.4	
(C20–N22)	1.342	1.333	1.339	(C7–C8–F10)	109.5	112.4	
(N22–C23)	1.452	1.468	0.413	(C7–C8–F11)	109.5	110.0	
(C23–C24)	1.530	1.514	1.497	(F9–C8–F10)	109.5	107.1	
(C23–H37)	1.090	1.089	0.980	(F9–C8–F11)	109.5	106.7	
(C23–H38)	1.090	1.084	0.970	(C8–F9–H25)	101.7	99.5	
(C24–H39)	1.090	1.090	0.970	(F10–C8–F11)	109.5	108.0	
(C24–H40)	1.090	1.092	0.980	(C14–C13–C18)	120.0	118.4	119.30
(C24–H41)	1.090	1.093	0.980	(C13–C14–C15)	120.0	120.8	119.30
				(C13–C14–H30)	120.0	119.8	120.30
RMSD (Å)	0.0739	0.0784		RMSD (°)	0.6164	1.5570	

a*- from reference 23 and 24.

46.36 ppm) and C24 (exp-21.58 ppm, theo-22.46) atoms. The ^{1}H chemical shifts of ETP5C were calculated in the region around 0.866–9.051 ppm experimentally and 1.281–9.172 ppm theoretically. In ETP5C, 17H atoms (with ring, NH, OH, FH, CH_2 and CH3 group). The hydrogen atoms in the methyl groups such as –CH_3═C24–H39–H40–H41, –CH_3═C19–H34–H35–H36 possesses low chemical shifts. The hydrogen atoms in methylene group exhibiting shifts higher than the methyl group hydrogen atoms. The hydrogen atoms with electro negative atoms exhibiting shift in the range of 4–7 ppm. The ring hydrogen atoms (H30–H33) possess high chemical shifts. The RMSD values of C13 and ^{1}H NMR are calculated at 0.6233 ppm (C13) and 0.5483 ppm (^{1}H) for title molecule.

3.4. Mass spectra and elemental analysis

The mass spectrometry data for the examined compound provides valuable insights into its molecular structure and fragmentation behaviour. To identification elemental analysis and mass spectra as shown in Figs. 6 and 7. The base peak at *m/z* 362, the most prominent ion, indicates a specific fragment's removal from the molecule, aiding in understanding its composition. Several significant peaks reveal structural details:*m/z* 346: Loss of an OH group (hydroxy group) signifies the departure of a hydroxy group atom. *m/z* 294: Elimination of a trifluoromethane radical suggests the aremoval of a specific substituent group. Intense peaks at *m/z* 290 and 332 indicate substantial structural changes:*m/z* 332: Removal of a sulphur atom (S) implies a specific structural alteration. *m/z* 290: Elimination of a CH3CH2COOCH3 radical signifies another significant structural modification. Notable peaks at *m/z* 92 (tropilium ion), 88 (propionic acid), 69 (CF3), 77 (thio urea moiety), and 18 (water) suggest the presence or fragmentation of distinct functional

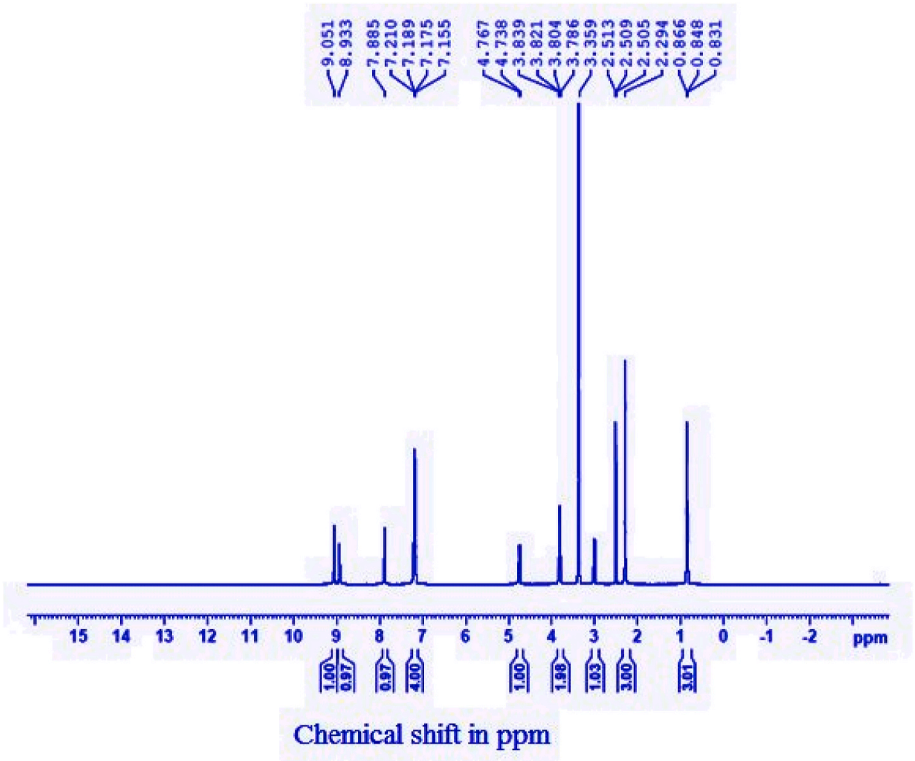

Fig. 4. Nuclear Magnetic Resonance spectrum (^{1}H) of ETP5C.

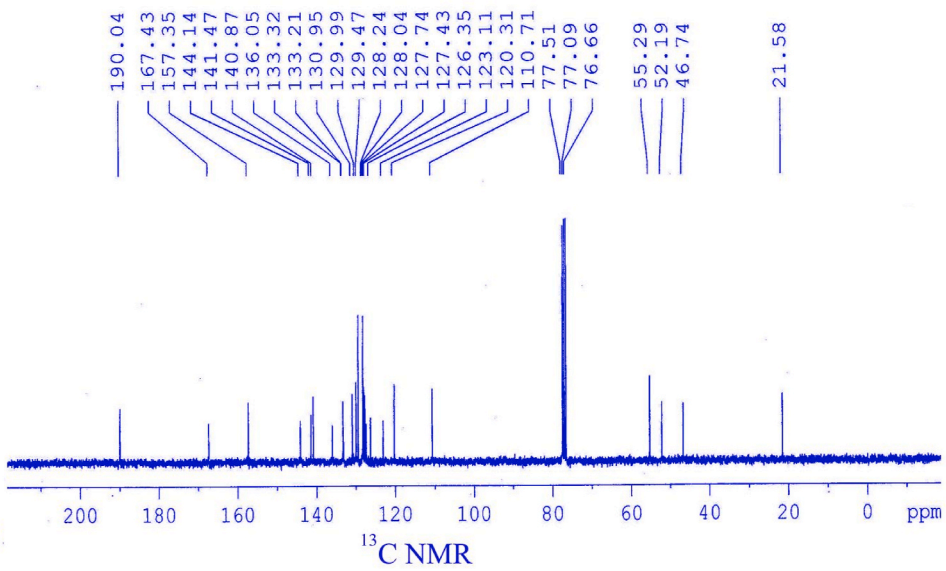

Fig. 5. Nuclear Magnetic Resonance spectrum (C_{13}) of ETP5C.

groups. The peak at *m/z* 272 reveals a fragment resulting from the removal of the toluene moiety, providing insights into the compound's structure. This mass spectrometry data is crucial for identifying complex molecules in fields like organic chemistry, pharmaceuticals, and analytical chemistry, where understanding fragmentation patterns aids in structural elucidation and compound identification.

Table 2
Chemical shift values of C_{13} Nuclear Magnetic Resonance of ETP5C (experimental, theoretical in ppm).

Atom	Chemical shifts (ppm)	
	Experimental	B3LYP/6–311++G (d,p)
C5	190.04	189.91
C20	167.43	168.23
C8	157.35	157.55
C16	144.14	143.93
C14	141.17	142.44
C13	140.87	140.59
C17	129.47	129.51
C18	127.43	126.74
C15	126.35	125.32
C2	77.51	77.32
C23	76.66	77.14
C3	55.79	55.04
C7	52.19	51.86
C19	46.74	46.36
C24	21.58	22.46
RMSD	0.6233	

Table 3
Chemical shift values of ^{1}H Nuclear Magnetic Resonance of ETP5C (experimental, theoretical in ppm).

Atom	Chemical shifts (ppm)	
	Experimental	B3LYP/6–311++G (d,p)
H30	9.051	9.172
H32	8.933	9.013
H31	7.885	7.756
H33	7.210	7.210
H27	7.189	6.887
H28	7.175	6.822
H29	7.155	5.038
H26	4.767	4.776
H37	4.738	4.613
H38	3.839	3.880
H25	3.821	3.812
H34	3.804	3.795
H35	3.786	3.765
H36	2.513	2.378
H40	2.509	2.252
H39	2.505	2.187
H41	0.866	1.281
RMSD	0.5483	

3.5. Vibrational (FTIR) spectral analysis

The ETP5C is a non-linear small molecule which has $C_{15}H_{17}F_3N_2O_3S$ (41 atoms) molecular formula with the molecular weight of 362.3661 g/mol. These 41 atoms have 117 degrees of freedom in it for the vibrations. The molecule has 3 hydrogen bond donors and 6 hydrogen bond acceptors in it. The molecule has two methyl groups with triflurometh‌yl group at C8–F9–F10–F11. The vibrational assignments have been made theoretically for FT-IR to compare with the experimental data of the same. Firstly, the assignment was performed tentatively on the basis of unscaled frequency values and then they are scaled by appropriate scaling factor (0.961) which is less than one [26]. The data of scaled and experimental frequencies are in agreement with each other. The assignments of fundamental vibrational modes of ETP5C with its intensities have been given in detail in Table 4. The wavenumber values, scaled frequencies by unscaled values, intensities of IR, PED have been obtained by VEDA program. The comparison graph between theoretical experimental FT-IR has been shown in Fig. 8.

3.5.1. N–H: vibrations

Generally, a hydrogen bond is often called as partial intermolecular bond between a lone pair of a given molecule on a nucleophilic atom (donor-electron rich) and hence N–H bond is produced. The γ N–H (stretching) vibrations are produced in the higher frequency regions and bending vibrations are produced at the lower frequency regions with low energies. The pymiridine ring produce γ N–H vibrations at 3497-3089 cm^{-1} due to the anti-bonding of H and electronegative N atom [27] which is higher than any other stretching

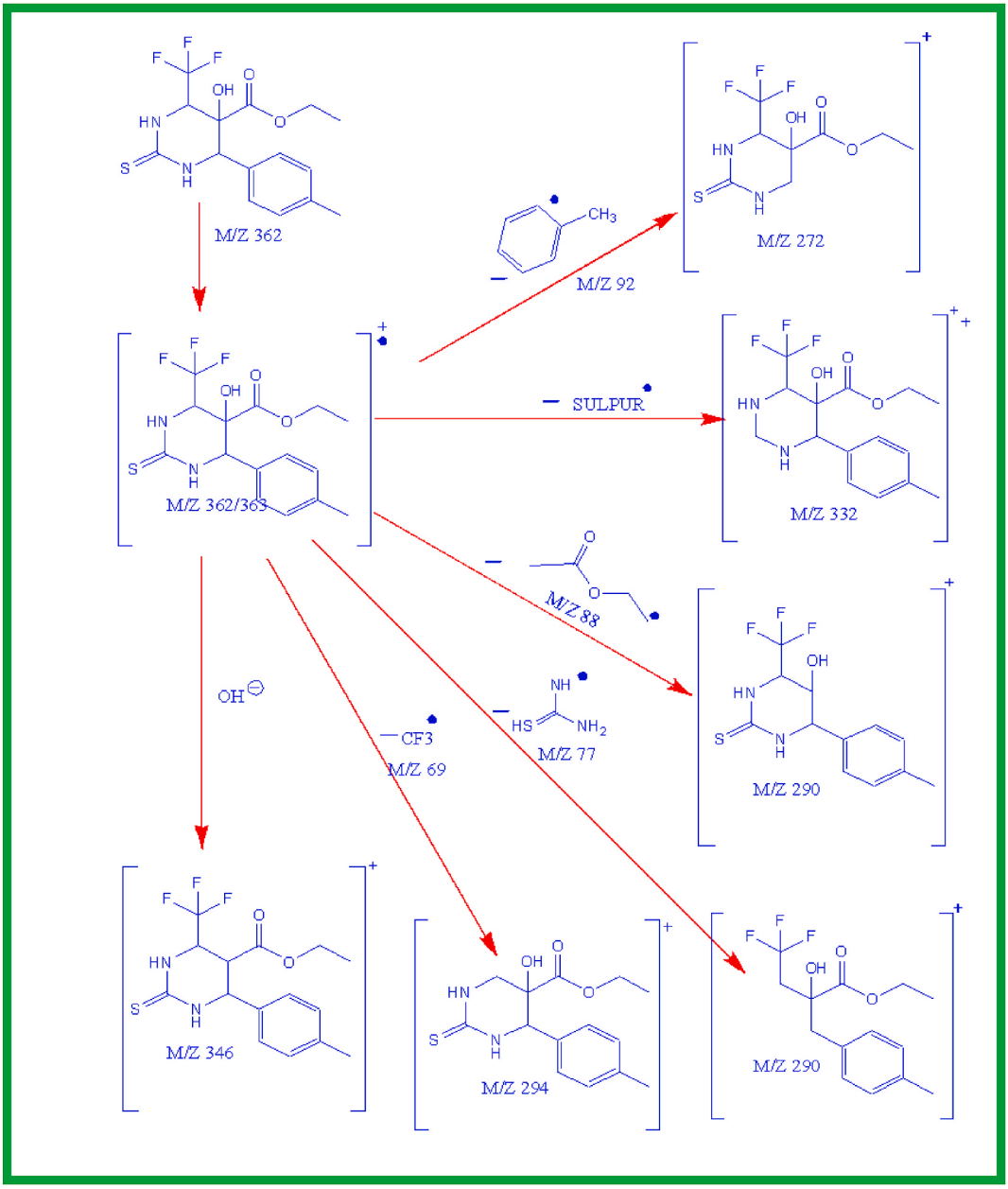

Fig. 6. Elemental analyses of title molecule.

frequencies. The molecule ETP5C has γ N–H vibration at 3388 cm^{-1} experimentally in FT-IR and 3359, 3354 cm^{-1} theoretically. Potential Energy Distribution was attained as 92 % which confirms the N–H stretching. The experimental γ N–H value is in agreement with the theoretical value.

3.5.2. O–H: vibrations

The vibrations of γ O–H generally occurred around 3500 cm^{-1} [28], which is most sensitive vibrations and hence it shows shifts in the FT-IR spectrum. It bands of weak intensity in FT-IR at 3246 cm^{-1} experimentally, at the same time theoretically obtained at 3247 cm^{-1} with the 100 % of PED which confirms the O–H stretching. The experimental value is agreed with the theoretical value.

3.5.3. 3. C–H: vibrations

This stretching vibration is generally present at 3100–3000 cm^{-1} in aromatic heterocyclic compounds. This depends upon C═C bonds and orientation of the substituents [9,14,29]. D. Durga devi et al. [27], reported FT-IR spectra of C–H vibrations at 2956 cm^{-1}. Trocia N. Clasp et al. [30], reported Ethyl C–H vibrations of FT-IR spectra between 2975 and 2880 cm^{-1}. The C–H stretching ring

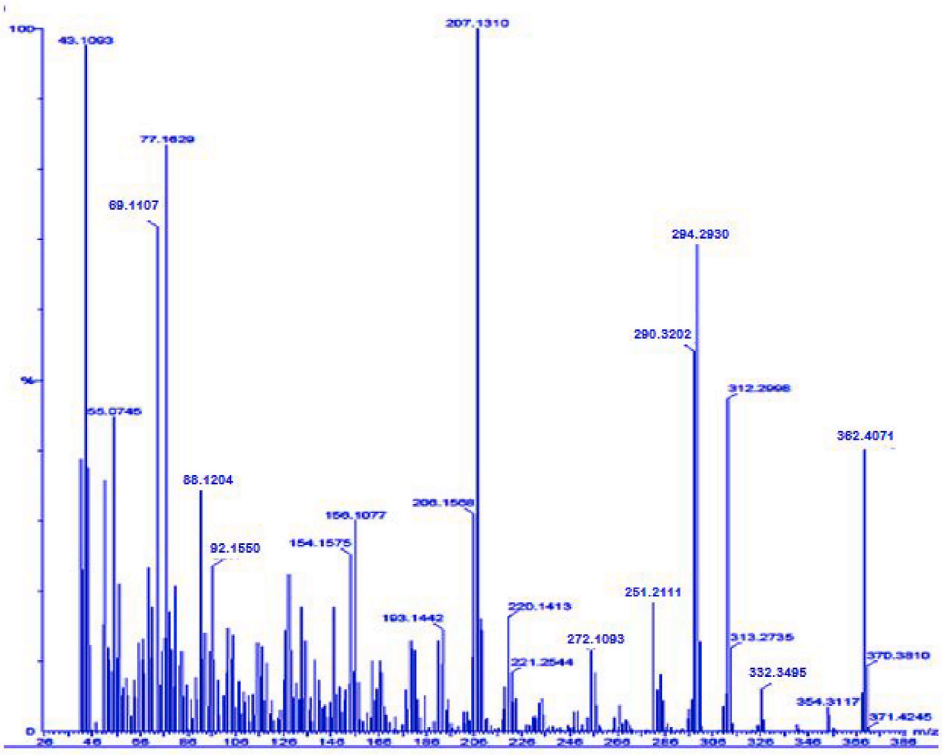

Fig. 7. Mass spectra of title molecule.

vibrations are falls at 3130-3107 cm^{-1} and 3052, 3043, 3006, 2996 cm^{-1} and observed experimentally at 3246 and 3026 cm^{-1}. The scaled theoretical values of ring C–H stretching mode agree well with that of experimental data as listed in Table 4. The molecule ETP5C has FT-IR bending H–C–C vibrations at 1418, 1341, 1178, 1016 and 772 cm^{-1} experimentally and 1416, 1345, 1176, 1013 and 773 cm^{-1} theoretically with the PED of 52, 74, 64, 58 and 51 %. It is confirmed that both experimental and DFT values are agreement with each other.

3.5.4. *Methylene (CH_2) group vibration*

For the vibration assignment of the CH_2 group, basically six fundamental modes can be assigned to each CH_2 group, namely the symmetric stretching, the asymmetric stretching, the scissoring mode and the rocking mode, which belong to the in-plane vibrations. In addition to those wagging and twisting modes of the CH_2 group are expected to belong to the out-of-plane symmetry modes. The C–H stretching of the methylene group is at lower frequencies than that of the aromatic C–H ring stretching. The asymmetric CH_2 stretching vibrations are usually observed in the region 3000-2900 cm^{-1}, while the symmetric CH_2 stretching occurs between 2900 and 2800 cm^{-1}. In this study, the bands observed at 3070 and 2983 cm^{-1} were assigned to the asymmetric and symmetric CH_2 vibrations in the FT-IR spectrum and theoretically calculated at 3057 and 2979 cm^{-1}. The calculated PED proves that the CH_2 stretching modes are pure modes contributing almost 100 %, as shown in Table 4. The deformation vibration of CH_2 calculated at 1434 cm^{-1}, contributes 80 % to the PED. The wagging vibration of CH_2 is observed at 1396 cm^{-1} and calculated at 1378 cm^{-1}. The rocking and twisting vibrations are calculated at 1257 and 961 cm^{-1} respectively.

3.5.5. *Methyl (CH_3) group vibrations*

The title compound ETP5C possesses two CH_3 groups, one in the ethyl group and another one in the benzene group. The vibrations of each CH_3 system in the title molecule should be expressed by 12 normal modes. The nine modes can be described as three stretching modes; two γ_{as}-asymmetric and one γ_s - symmetric; three bending modes; two asymmetric deformations (asymd) and one symmetric deformation (symd); two rocking modes and one torsional mode of the CH_3 group. The remaining three modes describe the vibrations of the entire C–CH_3 group, which has two bending and one stretching mode of the C–CH_3 bonds. The C–H stretching in the CH_3 group occurs at lower frequencies than the aromatic C–H stretching (3100-3000 cm^{-1}). The first results from the asymmetric stretching of the CH_3 mode, in which the two C–H bonds of the method group expand while the third shrinks. The second results from the symmetric stretching, in which all three C–H bonds expand and shrink in-phase. The asymmetric stretching of CH_3 is stronger than the symmetric stretching. In the present study, the asymmetric CH_3 stretching vibration, which appears in FT-IR at 3026 cm^{-1} is assigned to both groups of CH_3 asymmetric stretching vibration. The values at 3036 and 3032 cm^{-1} (mode nos. 107 and 106) expected theoretically by the B3LYP/6–311++G (d,p) method are in agreement with the experimental observations. The symmetric stretching mode of the CH_3

Table 4
FT-IR spectrum values with its vibrational assignments of ETP5C.

Mode no	Wave number (cm^{-1})			I_{IR}[c]	Assignments (PED)[a]
	Experimental	Theoretical			
	FTIR	Unscaled	Scaled[b]		
117	3388(m)	3495	3359	8	γ NH(92)
116	–	3490	3354	38	γ NH(92)
115	3246(w)	3378	3247	28	γ OH(100)
114	3246(w)	3257	3130	1	γ CH(87)
113		3251	3124	6	γ CH(87)
112		3240	3114	2	γ CH(94)
111		3233	3107	3	γ CH(97)
110	3070(w)	3181	3057	8	γ_{as} CH_2(94)
109		3176	3052	4	γCH(98)
108	3026(w)	3166	3043	4	γCH(99)
107	3026(w)	3160	3036	4	γ_{as} CH_3(99)
106	3026(w)	3155	3032	1	γ_{as} CH_3 (94)
105	3026(w)	3128	3006	2	γ CH(100)
104	3026(w)	3117	2996	3	γ CH(99)
103	2983(w)	3100	2979	3	γ_s CH_2 (99)
102	2965(w)	3085	2965	3	γ_s CH_3(99)
101	2945(w)	3076	2956	8	γ_s CH3(99)
100	1720(s)	1837	1765	59	γ OC (90)
99		1715	1648	2	γ CC(61)+β HCC(12)
98		1699	1633	0	γ CC(61)
97	1543(s)	1601	1539	41	γ CC(74)
96		1590	1528	4	γ CC(10)+β HCN(26)
95	1485(s)	1521	1462	1	asymd CH_3 (86)
94		1505	1446	4	β HCC(34)
93		1502	1444	1	β HCO(68)
92		1499	1440	1	β HCC(85)
91		1492	1434	1	deformation CH_2(80)
90		1481	1423	100	asymd CH_3 (41)
89	1418(m)	1474	1416	1	β HCC(52)
88	1396(m)	1434	1378	2	ω- CH_2 (62)
87	1375(m)	1419	1364	6	symd CH_3 (48)+γ CC(32)
86		1403	1348	10	β HOC(53)
85	1341(s)	1400	1345	0	β HCC (74)
84		1390	1336	11	β HOC(58)
83		1372	1318	4	β HOC(39)
82	1311(m)	1364	1311	7	β HCN(68)
81		1355	1302	31	β HCN(43)
80		1333	1281	54	β HCN(41)
79		1308	1257	0	r-CH_2(14)
78		1300	1249	0	γ_{as} COO(73)
77	1235(m)	1289	1239	42	β HOC(43)
76	1235(m)	1268	1219	0	γ CC(23)
75	1192 (vs)	1245	1197	35	γ CC(59)+β HNC(32)
74		1239	1191	4	γ CC(15)+β HNC(37)
73		1225	1177	21	β HCN(20)
72	1178 (vs)	1224	1176	1	β HCC(64)+γ CC(12)
71	1126(s)	1176	1130	1	β HCO(80)
70	1126(s)	1165	1120	5	β HCC(53)
69	1126(s)	1146	1101	10	γ_s COO (15)+ γ CC(38)
68		1142	1098	4	γ_{as} CF_3(37)
67	1086(s)	1131	1087	1	β HNC(23)+ γ_{as} CF_3 (26)
66	1086(s)	1120	1076	45	γ CC(27)+β HNC(11)
65	1048(m)	1081	1039	81	γ CC(39)
64		1072	1030	29	r CH_3 (43)
63		1066	1024	5	γ_s CF_3 (57)
62	1016(s)	1054	1013	3	r CH_3 (58)
61		1052	1011	28	γ CC(70)
60		1032	992	4	γ CC(46)
59		1025	985	1	τ HCCC(50)
58	975(m)	1001	962	6	γ CC(63)
57		1000	961	17	t-CH_2(56)
56		982	944	0	τ HOCC(68)
55		968	930	0	τ HCCC(11)+ τ HNCS(17)
54	903(m)	962	925	9	γ CC(33)
53	847(m)	890	855	7	γ CC(28)

(*continued on next page*)

Table 4 (*continued*)

Mode no	Wave number (cm^{-1})			I_{IR}[c]	Assignments (PED)[a]
	Experimental	Theoretical			
	FTIR	Unscaled	Scaled[b]		
52		884	850	5	β HCC(14)
51		853	819	1	τ HCCC(19)
50	810(s)	847	814	1	τ HCCC(54)
49		824	792	14	γ CC(36)
48		818	786	5	τ HCCC(47)
47	772(m)	804	773	0	β HCC(51)
46		799	768	1	γ CC(32)
45		790	759	3	β HNC(12)+γ CC(49)
44	741(m)	763	733	1	τ HCCC(36)
43	707(s)	740	711	3	τ HCCC(75)
42		704	676	2	β HCN(12)
41	644(m)	656	631	0	γ CS(75)
40	610(s)	630	606	1	asymd CF_3(43)
39		620	596	2	τ HOCC(12) + deformation in COO(24)
38	576(m)	597	574	1	γ CC(14) + asymd CF_3(32)
37		582	559	11	τ HNCC(74)
36		562	540	3	β CNS(10)
35	504(s)	513	493	3	ω –COO(44)
34		505	486	1	τ HCCC(31)
33	474(m)	492	473	3	τ HCCC(14)+β HNC(26)
32	448(m)	462	444	4	symd CF_3 (29)
31		433	416	6	r COO(22)
30	404(m)	423	407	2	β CCC(48)
29	–	409	393	2	τ HCCC(37)+β HNC(12)
28	–	381	366	0	β HNC(23)
27	–	371	356	1	r CF_3 (47)
26	–	352	338	1	r CF_3 (12)+β HNC(11)
25	–	329	316	4	β HNC(46)
24	–	322	309	4	β HCC(25)+ τ HOCC(10)
23	–	314	302	0	γ CC(17)
22	–	293	282	0	β CNS(11)
21	–	288	277	3	β HCC(19)
20	–	286	275	3	τ HOCC(25)
19	–	250	240	9	τ HOCC(10)
18	–	241	231	5	τ HOCC(11)+ τ HCOC(11)
17	–	221	212	0	τ HCOC(13)
16	–	207	199	1	τ HOCC(11)
15	–	198	191	5	τ HOCC(12)
14	–	180	173	1	τ HOCC(28)
13	–	164	158	1	β HCN(21)+ τ HOCC(15)
12	–	138	132	1	τ HCCC(66)+ τ HOCC(10)
11	–	107	103	0	β HCC(26)
10	–	103	99	0	τ CH_3(12)
9	–	92	89	1	τ HCCC(21)
8	–	77	74	0	τ HCCC(34)+ τ HNCC(10)
7	–	63	61	0	τ HCCC(34)
6	–	60	58	0	t COO(21)
5	–	55	53	0	τ HOCC(22)
4	–	45	43	0	β HCC(10)
3	–	37	36	0	τ HCOC(15)
2	–	29	28	39	τ CH_3 (23)
1	–	15	15	1	τ HNCN(13)+ τ HNCC(60)

[a] γ-stretching,γ_a-Symmetrical stretching,γ_{as}-asymmetrical stretching, β-bending, τ-torsion, ω-wagging, t-twisting, r-rocking, symd-symmetric deformation asymd-asymmetric deformation, vs-very strong, s-strong, m-medium, w-weak.

[b] Scaling factor: 0.961 for B3LYP/6-311 + G (d,p).

[c] Relative absorption intensities normalized with highest peak absorption equal to 100.

groups is observed at 2965 cm^{-1} (mode no. 102). For the methyl-substituted benzene derivatives, the asymmetric and symmetric deformation vibrations of the methyl group generally occur in the ranges 1465-1440 cm^{-1} and 1390-1370 cm^{-1}, respectively. Based on the above literature data, the medium strength band at 1485 cm^{-1} observed in the FT-IR spectrum is assigned to the asymmetric CH3 deformation vibration in the present study. In our calculations, the asymmetric deformation vibrations are predicted in the range of 1462 and 1423 cm^{-1} (mode nos. 95 and 90). The value at 1364 cm^{-1} (mode no. 87) calculated theoretically by the B3LYP/6–311++G (d,p) method is assigned to the symmetric deformation vibration in the CH_3 groups, which is also consistent with the above literature data as well as the FT-IR spectrum. The rocking vibrations of the CH_3 group of both CH_3 units appear as independent

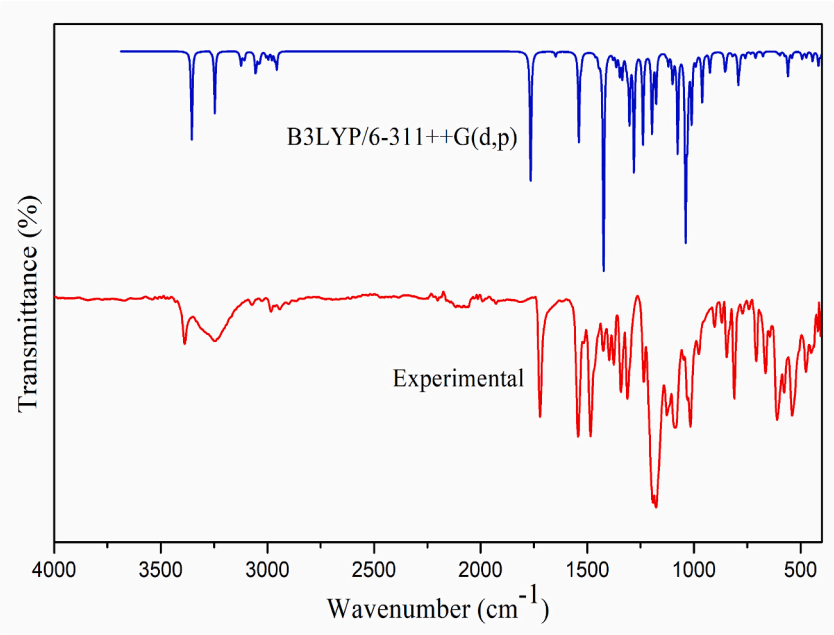

Fig. 8. FT-IR spectrum of ETP5C (Theoretical, Experimental).

vibrations. These vibrations normally occur in the range 1070–1010 cm^{-1}. In comparison with the above literature data, the band at 1016 cm^{-1} observed in the FT-IR spectrum is assigned to the CH_3 rocking vibration. The theoretically predicted values at 1030 and 1013 cm^{-1} (mode nos. 64 and 62), which are assigned to the CH_3 rocking vibration are in exact agreement with both the literature and the recorded FT-IR spectrum. Since CH_3 torsion modes below 100 cm^{-1} are expected, the calculated wavenumbers at 99 and 39 cm^{-1} (mode nos. 10 and 2) are assigned to the CH_3 torsion mode. These modes are not pure as evident from Table 4.

3.5.6. *Ester group of vibrations*

M. Minteguiaga et al. reported FT-IR spectra of carbonyl C═O stretching mode is around 1740 cm^{-1} [31], in our compound for C═O (C20–O21) observed in FT-IR spectra at 1720 and 1765 cm^{-1} theoretically with the PED of 90 %. Methyl ester has the strong absorption bands over the C–O asymmetric stretching modes at 1315-1195 cm^{-1} and the symmetric stretching modes at 1096-900 cm^{-1}. The theoretically calculated wavenumber at 1249 and 1101 cm^{-1} (mode no. 78 and 69) is assigned to the asymmetric and symmetric stretching modes with a PED of 73 and 15 %, respectively. The calculated wavenumber at 596 cm^{-1} (mode no.39) is assigned to the deformation in COO. The band at 504 cm^{-1} in the FT-IR spectrum and 493 cm^{-1} in the DFT spectrum is assigned to wagging mode. The computed wave number at 416 and 58 cm^{-1} (mode nos. 31 and 6) are assigned to the rocking and twisting mode of CO–O. The observed and calculated data of this vibration is coincidence which has been shown in Table 4.

3.5.7. *C - C: vibrations*

D. Durga devi et al. [27], reported FT-IR spectra of C–C vibrations of pyrimidine between 1392 and 904 cm^{-1}. The present study γCC vibrations are observed at 1126, 1086 cm^{-1} and calculated at 1101, 1076 cm^{-1} with 38, 27 % of PED. In ring of organic compounds, vibrations of γ C═C and γ C–C are lie at 1625-1430 cm^{-1} and 1380-1280 cm^{-1} respectively [32,33]. The γ C═C of ETP5C observed in FT-IR spectra at 1543 cm^{-1} and 1539 cm^{-1} and theoretically with PED of 74 %. The ring γ C–C (stretching) vibrations is observed at 1396, 1375, 1325 in FT-IR spectra and estimated at 1378, 1364 cm^{-1} with 62, 32 % of PED and other C–C stretching vibrations of ETP5C have been observed at 1192,1178, 1048,975,903,847 cm^{-1} and calculated at 1197, 1176, 1039, 962, 925, 855 cm^{-1} with 63 % PED. The vibration of β C–C–C in ring observed at 404 cm^{-1} as a medium intensity band and estimated as 407 cm^{-1} with the PED of 48 %. The other theoretical C–C vibrations are listed in Table 4.

3.5.8. *CF_3 group vibrations*

The title compound ETP5C contains a CF_3 group attached with one carbon atom of the pyrimidine ring. The fundamental vibrations associated with the CF_3 group are two asymmetric stretching, one symmetric stretching, two asymmetric deformations, one symmetric deformation, two rocking and one twisting modes. The bands at 1086 cm^{-1} observed in FT-IR correlate well with the values at 1098 and 1087 cm^{-1} calculated by B3LYP, which are assigned to the asymmetric C–F stretching and the band at 1024 cm^{-1} to the symmetric C–F stretching vibration. The intermediate intensity peaks at 610 and 576 cm^{-1} in the FT-IR spectra of ETP5C confirm the presence of asymmetric deformation vibrations of CF_3 and the calculated values at 606 and 574 cm^{-1} correlate well with the experimental data and the literature data [34,35]. The experimental peak at 448 cm^{-1} confirms the presence of the symmetric deformation mode of the CF3 group and the calculated value is 444 cm^{-1} (mode no. 32). The CF_3 rocking mode normally occurs in the range of 450–350 cm^{-1}

and 350-260 cm^{-1} [36]. The value at 338 and 356 cm^{-1} calculated by the B3LYP method is assigned to CF_3 in-plane and CF_3 out-of-plane rocking, respectively. Due to the low wavenumber, it is difficult to observe the torsion motion in the FT-IR spectra.

3.5.9. C–S vibration

Generally the C–S stretching bands lie in the range 930–670 cm^{-1} [28] with a moderate intensity. In the present study, the computed wave number at 631 cm^{-1} is designated as C–S stretching vibration and comparable to observed vibration at 644 cm^{-1}. The C–S in-plane and out-of plane bending vibrations are lying in the regions 600- 420 cm^{-1} and 420-320 cm^{-1}, respectively [37]. In ETP5C, the calculated frequency at 540 cm^{-1} and 282 cm^{-1} by DFT method gives the C–S in plane and out-of-plane bending vibration, respectively.

3.5.10. Other vibrations in ETP5C

The vibrations of β H–C–O bending observed in FT-IR spectra at 1235, 1126 cm^{-1} in which 1126 cm^{-1} has strong peak. The bending H–C–O vibrations (β) are calculated theoretically at 1239, 1130 cm^{-1} with 86 %, bending H–C–N vibrations(β) observed in FT-IR spectra at 1311, 1192, 1086, 474 cm^{-1} at where 1192 cm^{-1} has very strong intensity peak, and also H–C–N bending vibrations (β) estimated theoretically at 1311, 1197, 1087, 473 cm^{-1} with PED of 68 %. The vibrations of τ H–C–C–C observed at 810, 741, 707, 474 cm^{-1} and estimated at 814, 733, 711, 473 cm^{-1} with PED of 75 %. The peak at 707 cm^{-1} has been obtained as strong intensity peak. The vibrations related to 117° of modes have been mentioned in detail theoretically in Table 4 along with the experimental values.

3.6. Electronic properties

The absorption characterization of ETP5C was found out experimentally by UV–Vis spectrum utilizing DMSO solvent and theoretically by TD-DFT/MO62X/6–311++G (d,p). The TD-DFT provides more accuracy than the other methods during the calculation of static/dynamic properties of the appropriate molecules particularly in excited states. The absorption spectrum of ETP5C has shown in Fig. 9 experimentally and theoretically as a combined spectrum. The estimated values of maximum absorption wavelength listed in Table 5 along with its energy, band gap, oscillator frequency and assignments. The absorption wavelength observed is 253 nm experimentally and 245 nm theoretically. The title molecule is observed for π to π* transition with major contributions are HOMO- > L+1 (36 %), HOMO- > L+5 (21 %) and HOMO- > LUMO (15 %) states. This value shows the number of electrons passed into the ring of the molecule.

The analysis using Frontier molecular orbitals was performed for ETP5C for different HOMO-LUMO energies by how the band gap values attained and also values are compared with the UV–Vis values and observed that good agreement. Table 5 depicts the maximum probability of the electronic transitions of ETP5C from HOMO to LUMO+1 as 36 % (E_g = 5.518 eV), from HOMO to LUMO+5 as 21 % (E_g = 3.6 eV) and from HOMO to LUMO as 15 % (E_g = 4.625 eV). These transitions of the molecule were observed and reported in Fig. 10. In addition, HOMO-1 to LUMO+1 as 33 % (E_g = 5.224 eV) and HOMO-1 to LUMO+5 (E_g = 3.727 eV) as 27 % have also shown in Fig. 10. HOMO-LUMO analysis plays a significant role in organic chemistry for the prediction and selection of many organic products. The word Frontier implies the outer surface of the molecule that can delocalize spatially to the higher energies [14,38]. Fig. 10 describes the various HOMO-LUMO orbitals. The delocalization takes place in these orbits by the interactions of the orbits. The green and blue circles in the molecule of Fig. 10 indicate the electron-hole pair. If electron gains sufficient energy, then it reaches LUMO from HOMO orbitals.

The density of states (DOS) is a function that describes the number of available states for occupation in a given system at every level of energy and tells about the carrier concentrations, energy distributions within the molecule [14,19]. The density of states of ETP5C

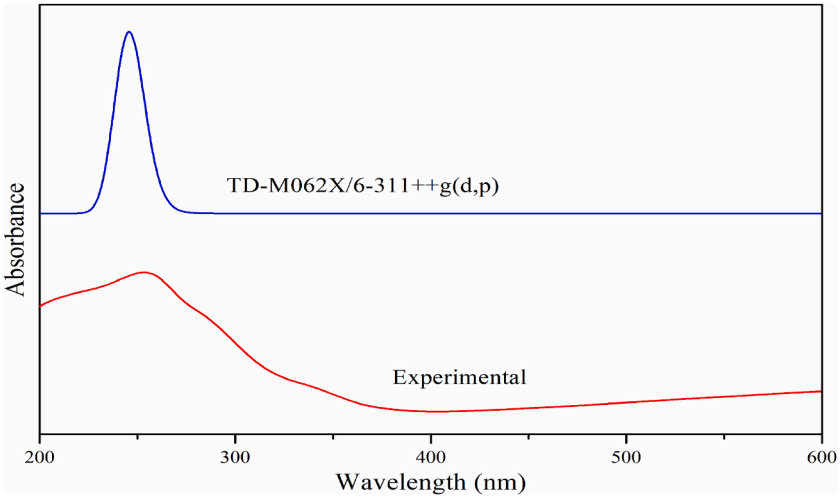

Fig. 9. UV–Vis spectrum of ETP5C (Theoretical, Experimental).

Table 5
UV–Vis maximum absorption wavelength of ETP5C (Experimental, theoretical).

Experimental		TD-DFT/6–311++G (d,p)				
λ_{max} (nm)	Band gap (eV)	λ_{max} (nm)	Band gap (eV)	Energy (cm^{-1})	f^{a}	Assignment
–	–	267	4.4878	36,069	0.0003	H-1- > L+1 (33 %), H-1- > L+5 (27 %)
–	–	261	4.7997	38,610	0.0076	H-5- > LUMO (3 %), H-5- > L+2 (4 %), H-5- > L+3 (6 %),
253	4.9135	245	5.0740	40,759	0.4182	HOMO- > L+1 (36 %), HOMO- > L+5 (21 %), HOMO- > LUMO (15 %

[a] - oscillator strength.

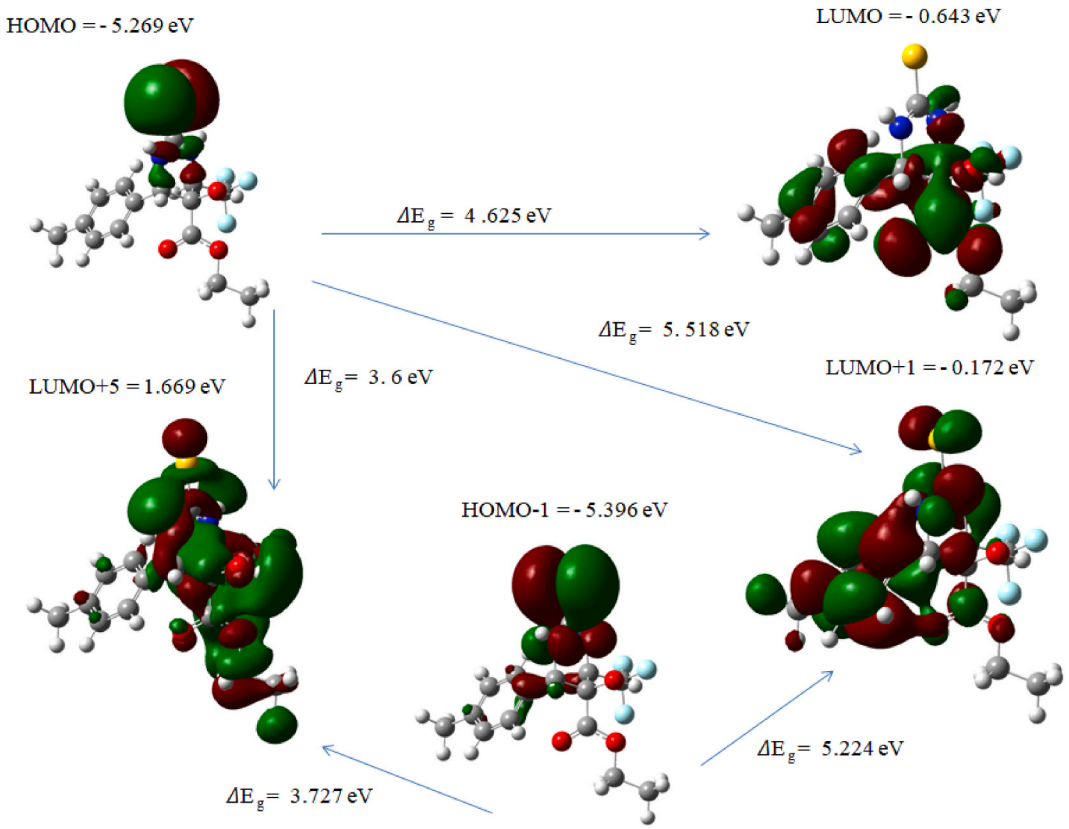

Fig. 10. HOMO-LUMO orbitals with the band gap values of ETP5C.

has been shown in Fig. 11 as total density of states (TDOS) and partial density of states (PDOS). In Fig. 11, black graph indicates the TDOS of the molecule, pink graph indicates the PDOS of carbon and hydrogen atoms of ETP5C, blue graph represents the fluorine atoms and red graph indicates the nitrogen, oxygen and sulphur atoms. The DOS of ETP5C is high and hence the occupation at each energy level is also high. The small straight pink with black lines depicts HOMO/filled orbitals and long dotted black line represents the band gap which separates the filled and unfilled orbitals of ETP5C. This energy gap is coincided with the energy gaps of FMO and UV–Vis analysis.

The parameters using HOMO-LUMO energy values were reported in Table 6. Since band gap value is small, easily delocalization takes place. During the localization and delocalization, the atom possesses chemical potential. These parameters explain the electronic and chemical behaviour of the organic molecule and hence this molecule can have importance in industrial (corrosion inhibitor, nonlinear optic materials, etc.) biochemistry and pharmaceutical field.

3.7. MEP, LOL and ELF analysis

Molecular Electrostatic Potential provides knowledge of relative polarity of a given molecule and helps to calculate the hydrogen bonding, the reactivity within the molecule, residual interaction of atoms, polarizability by dipole moment by molecules, drugs, organic compounds [39,40]. The electrostatic potential is the positive point charge energy of interaction with the given molecule. This potential is needed to bind the substrate and the sites of receptor in which the ligand and the receptor can latch each other at the

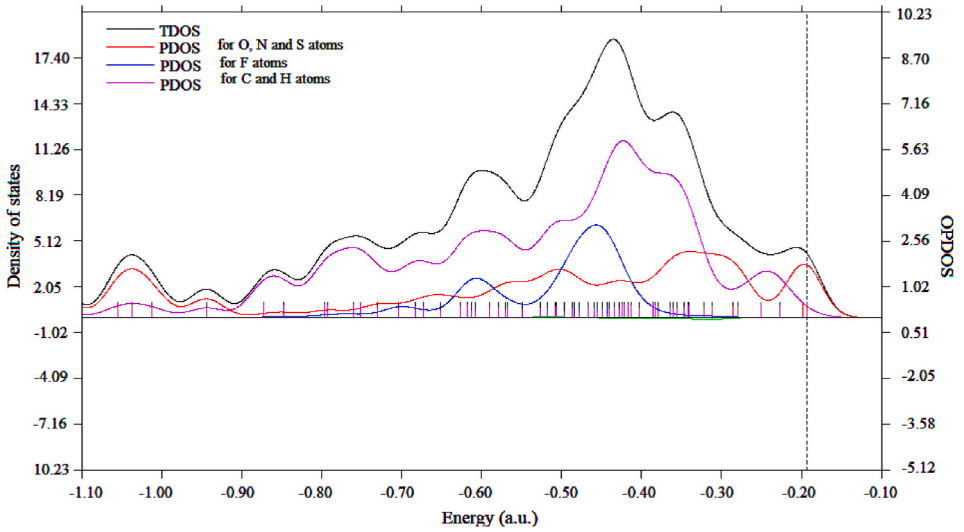

Fig. 11. Density of states (Total Density of States (TDOS), Partial Density of States (PDOS)) of ETP5C.

Table 6
Calculated energy values of ETP5C by B3LYP/6–311++G (d,p) method.

Parameters	B3LYP/6–311++G (d,p)
E_{Homo}(eV)	−5.2687
E_{Lumo}(eV)	−0.6432
Ionization potential	5.2687
Electron affinity	0.6432
Energy gap (eV)	4.6255
Electronegativity	2.9560
Chemical potential	−2.9560
Chemical hardness	2.3128
Chemical softness	0.2162
Electrophilicity index	1.8890
Electron donating capability (w-)	1.2781
Electron accepting capability (w+)	3.6561

surface of the molecule [41]. The reactive sites of electro and nucleophiles can be estimated by MEP for the molecule ETP5C using the theoretical method DFT/B3LYP/6–311++G (d,p) set with the software namely Gauss View 5.0. The MEP of ETP5C is visualized in Fig. 12 which shows the chemical and relative reactivity of the atoms of the molecule. The indicator bar that starts from red to blue code in the figure represents the electrophilic and nucleophilic regions of the ETP5C in which the potential increases from left to right. The value ranges from −0.05203 a. u to +0.05203 a. u. The negative regions (red, orange and blue) have been located on oxygen, nitrogen, fluorine and sulphur atoms of ETP5C that employ nucleophilic reactions. The positive regions (around blue) are located on hydrogen atoms that employ electrophilic reactions. These reactions conclude that the title molecule can have chemical and biological activities.

The topology analysis of ETP5C has been performed for LOL and the color filled plane map of the molecule has been shown in Fig. 13. The contribution of LOL atoms are important descriptor in chemical bonding [19]. The topological path shows the chemically significant region of the molecule in the figure. The red, orange and yellow color regions in the plane map show the LOL value with the path of the electron delocalization of the molecule. The relief and Electron Localization Function (ELF) color filled map was shown in Fig. 14a-c know the chemically significant area. The relief map connects every atom that has a peak (green in color) with its electronic environment (narrow peak within broad peak). The ELF color filled map shows the depletion layer between valence and inner shell in which a lone pair can be created [1,19]. Fig. 14a represents the map with carbon and a hydrogen atom, Fig. 14b represents the map for fluorine atoms and Fig. 14c represents map of nitrogen and oxygen atoms. The critical points, the path of the atoms connection, bond between atoms, chemically significant regions (due to electronegative atoms-red or orange regions around the nucleus) were shown in the color filled map. The region around lone pair particularly N & O atoms in ETP5C represented by blue color circle. The nucleus is represented by red point with blue circle that is covered by electronic environment and electrons are localized, red & orange represents chemically active sites which shown clearly in ELF map. This shows the charge shifting and chemical bonding with in the ETP5C molecule.

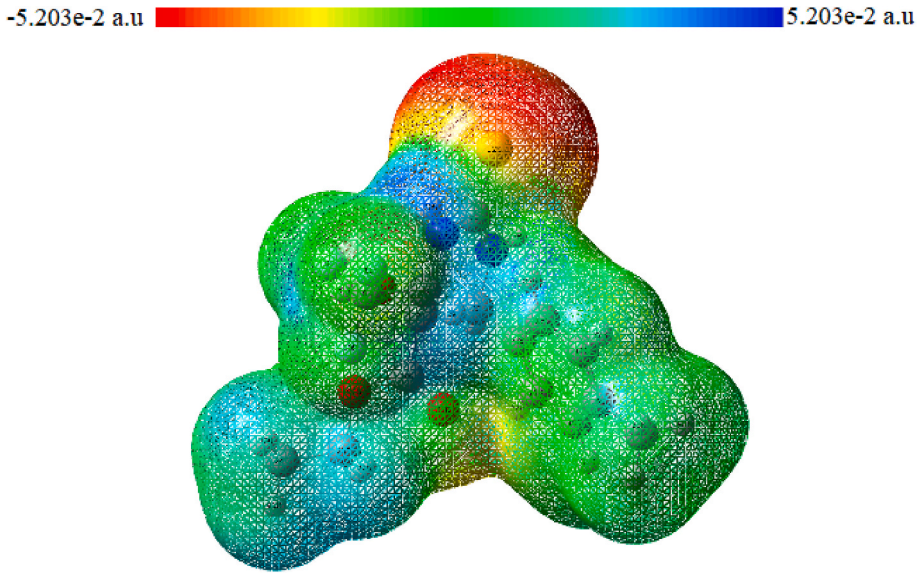

Fig. 12. The molecular electrostatic potential of ETP5C using the isodensity value is 0.0004 a. u.

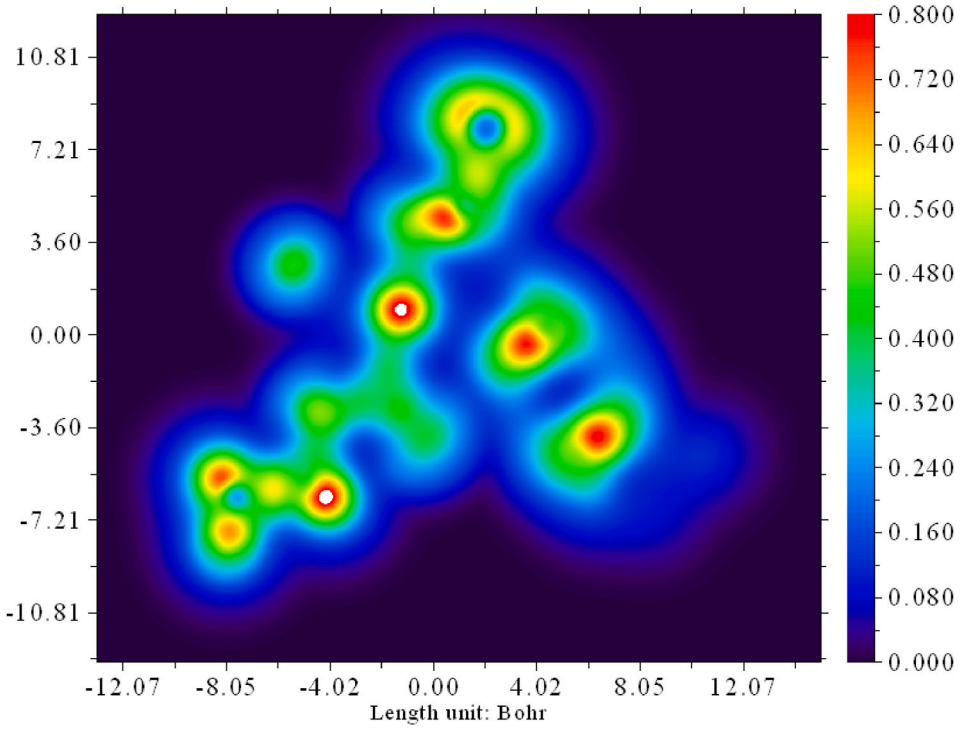

Fig. 13. Lol of ETP5C.

3.8. NLO analysis

The FMO analysis of ETP5C reports the dipole moment due to the charge delocalization of electrons from HOMO to LUMO orbitals. This internal charge transfer mechanism of ETP5C leads an important role to find the NLO properties. Nowadays, the organic compounds are used as an optical data storage devices, electronic devices, optoelectronic devices, sensors, solar cells etc when they are exposed to radiation [42–44]. The statement of Buckingham says that the DFT approach used for knowing the properties of NLO from reference [9]. These values decide the ability of the organic compound to have optoelectronic property, and the applications in the field of pharmacology and drug designing. The atoms share electrons unequally and hence the electronegativity differs. Due to this,

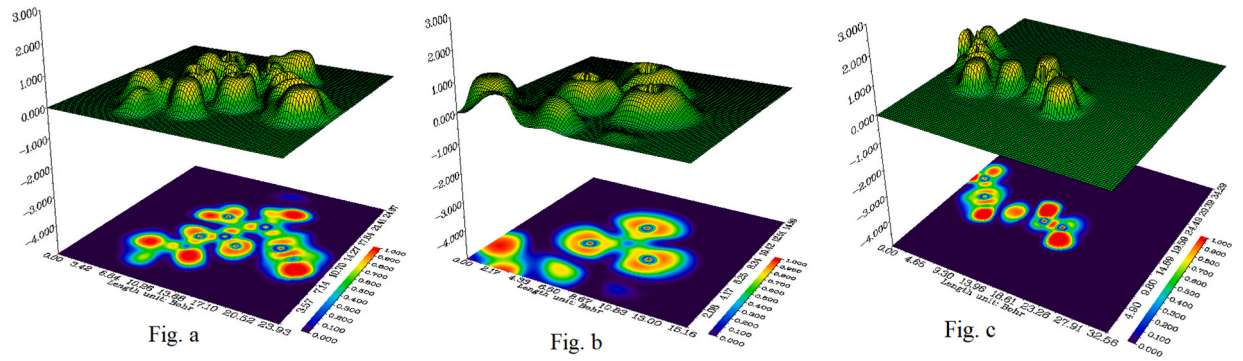

Fig. 14. ELF with Relief map of ETP5C.

dipole moment is produced based on its polarizability.

The values such as μ(D), α_0 and β_{tot} of ETP5C, calculated and listed in Table 7. The hyperpolarizability β_{tot} of ETP5C was calculated as $1.6662*10^{-30}$ e. s.u with the dipole moment value as 3.0040 D and the polarizabity value as $3.3665*10^{-23}$ e. s.u. These values have been calculated by above said method. The β_{tot} value of ETP5C was compared with the hyperpolarizability value of Urea (standard NLO reference $= 0.927 \times 10^{-30}$ e. s.u) [9]. The large β_{tot} value of ETP5C implies the potential of the molecule to reveal second order optical effects, due to intermolecular interaction in ETP5C which shown in ELF and LOL topology analysis of the molecule. Hence, the molecule ETP5C can have second order optical effects.

3.9. Local reactivity descriptors

An analysis of molecular reactivity generally performed using Fukui functions on the basis of electrophilic, nucleophilic and also by the free radical attacks within the molecule [45,46]. The NPA used to calculate the individual atomic sites of ETP5C molecule using B3LYP/6–311++G (d,p) basis set. The fukui function calculations have been made by the following equations [1–3].

$$f^{+}(\vec{r}) = q_r(N+1) - q_r(N) \text{ for nucleophilic attack} \quad (1)$$

$$f^{-}(\vec{r}) = q_r(N) - q_r(N-1) \text{ for nucleophilic attack} \quad (2)$$

$$f^{0}(\vec{r}) = \left(q_r(N+1) - q_r(N-1)\right) / 2 \text{ for radical attack} \quad (3)$$

where q_r denotes the atomic charge at rth atomic site which has been evaluated from NPA. N, N+1 and N-1 represents neutral, anionic and cationic chemical species, respectively. The nucleophilicity and electrophilicity are find out through dual descriptor which are calculated by the following equations [4]

$$\Delta f(\vec{r}) = f^{+}(\vec{r}) - f^{-}(\vec{r}) \quad (4)$$

The Dual descriptor reports $\Delta f(\vec{r}) > 0$ for the nucleophilic attack and $\Delta f(\vec{r}) < 0$ for the electrophilic attack. The MEP and ELF analyses have also been reported for nucleophilicity, electrophility and lone pairs due to electronegative atoms of ETP5C. The nucleophilic attack plays a major role on molecule when it is preferred in the field of biochemistry. The fukui function and dual descriptors values are reported in Table 8. The molecular reactivity and Dual descriptors are in agreement with the MEP and ELF analyses of the title molecule.

Table 7
The values of calculated dipole moment μ (D), polarizability (α_0), first order hyperpolarizability (βtot) components of ETP5C.

Parameters	B3LYP/6–311++G (d,p)	Parameters	B3LYP/6–311++G (d,p)
μ_x	−0.7561	β_{xxx}	246.8615
μ_y	−2.9027	β_{xxy}	136.8055
μ_z	0.1634	β_{xyy}	−121.4274
μ(D)	3.0040	β_{yyy}	−281.6662
α_{xx}	233.0077	β_{zxx}	12.4049
α_{xy}	−6.3868	β_{xyz}	−12.2340
α_{yy}	265.3994	β_{zyy}	35.4948
α_{xz}	11.8992	β_{xzz}	63.9950
α_{yz}	0.9842	β_{yzz}	108.6545
α_{zz}	183.0649	β_{zzz}	−49.5730
α_0 (e.s.u)	3.3665×10^{-23}	βtot (e.s.u)	1.6662×10^{-30}
Δα(e.s.u)	6.0751×10^{-23}		

Table 8
Fukui functions of ETP5C using NPA charges.

Atoms	NPA charges			Fukui functions			Δf(r)
	0,1 (N)	N +1 (-1,2)	N-1 (1,2)	fr +	fr -	fr 0	
O1	−0.73400	−0.75207	−0.72941	−0.01808	−0.00460	−0.01130	−0.01350
C2	0.18035	0.18199	0.18154	0.00164	−0.00120	0.00023	0.00283
C3	−0.03960	−0.03783	−0.05539	0.00174	0.01582	0.00878	−0.01408
N4	−0.60190	−0.59449	−0.53168	0.00745	−0.07030	−0.03140	0.07771
C5	0.31313	0.32819	0.29306	0.01506	0.02007	0.01757	−0.00501
N6	−0.63210	−0.63240	−0.58657	−0.00026	−0.04560	−0.02290	0.04531
C7	−0.12750	−0.14228	−0.13207	−0.01477	0.00456	−0.00510	−0.01933
C8	1.08642	1.07255	1.08562	−0.01387	0.00080	−0.00650	−0.01467
F9	−0.35990	−0.36710	−0.35227	−0.00719	−0.00760	−0.00740	0.00045
F10	−0.34830	−0.34401	−0.33491	0.00433	−0.01340	−0.00460	0.01776
F11	−0.35390	−0.36444	−0.34270	−0.01058	−0.01120	−0.01090	0.00058
S12	−0.29290	−0.35107	0.14620	−0.05820	−0.43910	−0.24860	0.38087
C13	−0.56990	−0.06824	−0.50844	0.50161	−0.06140	0.22010	0.56302
C14	0.58030	−0.12460	0.60508	−0.70490	−0.02480	−0.36480	−0.68012
C15	−0.44730	−0.23130	−0.43593	0.21600	−0.01140	0.10232	0.22737
C16	−0.03240	−0.03783	0.04523	−0.00542	−0.07760	−0.04150	0.07222
C17	−0.20120	−0.20858	−0.16375	−0.00743	−0.03740	−0.02240	0.02997
C18	−0.24550	−0.24339	−0.25197	0.00214	0.00644	0.00429	−0.00430
C19	−0.58340	−0.58226	−0.59654	0.00112	0.01316	0.00714	−0.01204
C20	0.80737	0.74988	0.80912	−0.05749	−0.00170	−0.02960	−0.05574
O21	−0.58950	−0.62277	−0.56679	−0.03325	−0.02270	−0.02800	−0.01052
O22	−0.55120	−0.56439	−0.53108	−0.01316	−0.02020	−0.01670	0.00699
C23	−0.02960	−0.04383	−0.03427	−0.01426	0.00470	−0.00480	−0.01896
C24	−0.58610	−0.60428	−0.58765	−0.01821	0.00158	−0.00830	−0.01979
H25	0.48914	0.45910	0.50109	−0.03004	−0.01200	−0.02100	−0.01809
H26	0.23736	0.19889	0.26153	−0.03847	−0.02420	−0.03130	−0.01430
H27	0.41780	0.40119	0.43000	−0.01661	−0.01220	−0.01440	−0.00441
H28	0.42214	0.39123	0.43290	−0.03091	−0.01080	−0.02080	−0.02015
H29	0.25613	0.22601	0.26609	−0.03012	−0.01000	−0.02000	−0.02016
H30	0.10532	0.17988	0.12629	0.07456	−0.02100	0.02680	0.09553
H31	0.19397	0.17704	0.21720	−0.01693	−0.02320	−0.02010	0.00630
H32	0.20237	0.17865	0.22035	−0.02372	−0.01800	−0.02090	−0.00574
H33	0.20915	0.19721	0.20526	−0.01194	0.00389	−0.00400	−0.01583
H34	0.21267	0.19739	0.23815	−0.01528	−0.02550	−0.02040	0.01020
H35	0.20521	0.17903	0.22056	−0.02618	−0.01540	−0.02080	−0.01083
H36	0.20464	0.17660	0.22302	−0.02804	−0.01840	−0.02320	−0.00966
H37	0.18568	0.09436	0.19210	−0.09132	−0.00640	−0.04890	−0.08490
H38	0.18597	0.13957	0.19027	−0.04640	−0.00430	−0.02540	−0.04210
H39	0.20597	0.15165	0.20930	−0.05432	−0.00330	−0.02880	−0.05099
H40	0.20495	0.13070	0.21035	−0.07425	−0.00540	−0.03980	−0.06885
H41	0.21074	0.10606	0.22348	−0.10468	−0.01270	−0.05870	−0.09194

3.10. Molecular docking analysis

The molecular docking (ligand-protein) is commonly used to predict the binding and interactions between small and macro molecule which leads to the treatment of various diseases in the field of molecular structural biology [47–49]. The values of Pa and Pi

Table 9
Molecular docking of ETP5C with Antineoplastic proteins.

Proteins	Bonded residues	No. of hydrogen bond	Bond distance (Å)	EIC (nm)	BE (kcal/mol)	IME (kcal/mol)	vdW + Hbond + desolv Energy	ESE (kcal/mol)	Reference RMSD (Å)
4IEX	LYS 89	4	2.6	170.70	−5.14	−6.93	−6.71	−0.22	15.12
	HIS 84		2.2						
	HIS 84		2.0						
	GLU 8		2.2						
5IEY	THR 198	3	2.0	759.57	−4.26	−6.05	−6.00	−0.05	20.771
	ARG 200		2.7						
	ARG 200		2.5						
1H7X	ALA 902	2	2.4	461.12	−4.55	−6.34	−6.40	0.06	146.797
	SER 316		2.6						
4EIV	ARG 127	3	2.3	127.00	−5.32	−7.11	−6.92	−0.18	14.35
	SER 131		2.6						
	SER 131		1.6						

EIC -Estimated Inhibition Constant, BE- Binding energy, IME -Intermolecular Energy, ESE-Electrostatic Energy.

named probability for active and inactive are known that predicts Pa >0.700 for a particular disease states that the molecule has an ability to react with the proteins that are used to cure the disease. ETP5C has Pa = 0.736, and Pi = 0.005 for antineoplastic activity that inhibiting the development of tumor cells. So antineoplastic proteins such as 4IEX, 5IEX, 1H7X and 4EIV were chosen from PDB and docking has been proceeded with the ligand ETP5C. The proteins have been docked with the ligand title molecule using Auto-dock/Auto grid software. The docking results of ETP5C with the selected proteins have been shown in Table 9 and the simulations have been shown in Fig. 15a-d. The bonded residues, number of hydrogen bonds, bond distances, estimated inhibition constant, binding energy, intermolecular energy, electrostatic energy have been reported in Table 8. These values suggest that ETP5C molecule may lead a significant role in antineoplastic to prevent the development of tumor cells. The minimum binding energies have been noted for ETP5C as −5.14 kcal/mol for 4IEX protein, as −4.26 kcal/mol for 5IEX protein, as −4.55 kcal/mol for 1H7X protein and −5.32 kcal/mol for 4EIV protein which denotes the stability of the molecule. Hence, ETP5C may have biological and pharmaceutical uses.

4. Conclusion

The synthesized organic title compound ETP5C molecule has gone through computational calculations. The vibrational spectral analysis FT-IR, spectral study of ^{13}C & ^{1}H NMR, mass spectra and UV–Vis. Spectra have been obtained and the results have been discussed with recorded spectral values. The potential energy surface (PES) emphasized the minimum energy stable conformer, molecular geometrical optimization and vibrational assigments modes with PED have been discussed in detail. By obtaining different HOMO-LUMO distributions for the molecule ETP5C, FMOs analysis explains how charges transform within the molecule. According to the findings, the maximum electronic distribution shows 36 % from orbital HOMO – LUMO+1 and 33 % from orbital HOMO-1 to LUMO+1. We have compared the HOMO-LUMO band gap value with the UV–Vis (E_g = 4.6255 eV). The TDOS, PDOS, MEP, LOL and ELF are used to visualize lone pair electrons, chemically active sites, bond critical points, nucleophilic and electrophilicsitesn in ETP5C. In addition, dual descriptor also explains the nucleo and electrophilic regions. The NLO properties of ETP5C have been estimated which states the second order optical effects. The docking analysis revealed that the molecule with antineoplastic proteins may prevent the development of tumor cells. This work increases the technology's applicicability in the preparation of novel biological chemical.

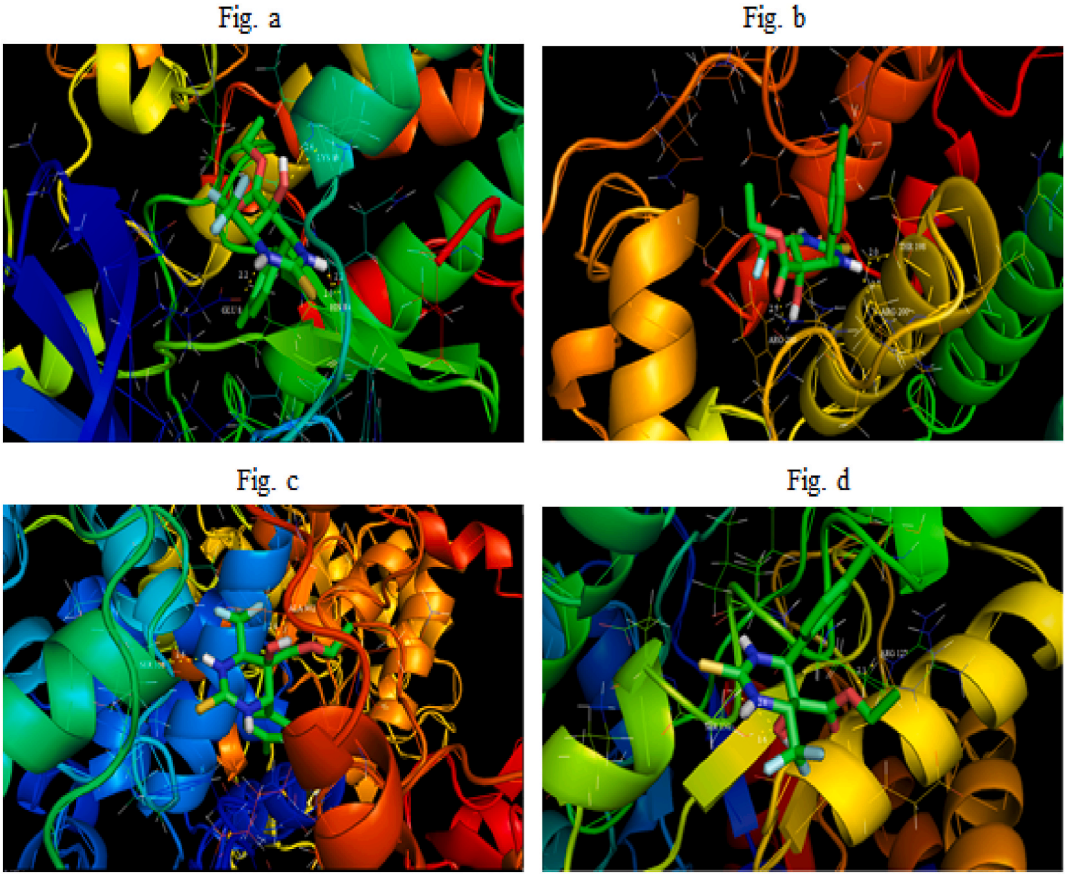

Fig. 15. Molecular docking of ETP5C with Antineoplastic ((a). 4IEX, (b). 5IEX, C. 1H7X and d. 4EIV) proteins.

Data availability statement

Data will be made available on request.

CRediT authorship contribution statement

I. Umadevan: Writing – review & editing, Writing – original draft, Visualization, Validation, Methodology, Conceptualization. **R. Rajasekaran:** Writing – review & editing, Supervision, Project administration, Investigation. **M. Anto Bennet:** Writing – review & editing, Validation, Methodology, Investigation, Formal analysis. **V. Rajmohan:** Writing – review & editing, Resources, Project administration, Investigation. **V. Vetrivelan:** Writing – review & editing, Validation, Supervision, Methodology, Conceptualization. **K. Sankar:** Writing – review & editing, Resources, Project administration, Investigation, Conceptualization. **M. Raja:** Writing – review & editing, Writing – original draft, Supervision, Resources, Project administration, Investigation, Conceptualization.

Declaration of competing interest

The authors declare that they have no known competing financial interests or personal relationships that could have appeared to influence the work reported in this paper.

References

[1] S. Aayisha, T.S. Renuga Devi, S. Janani, S. Muthu, M. Raja, S. Sevvanthi, B.R. Raajaraman, Vibrational and computational analysis for molecular structure properties of N-(2-(trifluoromethyl)phenyl)acetamide: density functional theory approach, Spectrosc. Lett. 52 (9) (2019) 563–576, https://doi.org/10.1080/00387010.2019.1678175.

[2] P. Zhan, X. Liu, Z. Li, Z. Fang, Z. Li, D. Wang, C. Pannecouque, E.D. Clercq, Novel 1,2,3- thiadiazole derivatives as HIV-1 NNRTIs with improved potency: synthesis and preliminary SAR studies, D. Bioorg. Med. Chem. 17 (2009) 5920–5927, https://doi.org/10.1016/j.bmc.2009.07.004.

[3] M. Bassetto, S. Ferla, F. Pertusati, Polyfluorinated groups in medicinal chemistry, Future Med. Chem. 7 (4) (2015) 527–546, https://doi.org/10.4155/fmc.15.5.

[4] C. Isanbor, D. O'Hagan, Fluorine in medicinal chemistry: a review of anti-cancer agents, J. Fluor. Chem. 127 (3) (2006) 303–319, https://doi.org/10.1016/j.jfluchem.2006.01.011.

[5] S. Purser, P.R. Moore, S. Swallow, V. Gouverneur, Fluorine in medicinal chemistry, Chem. Soc. Rev. 37 (2008) 320–330.

[6] F.J. Martins, C.A. Caneschi, M.P. Senra, G.S.G. Carvalho, A.D. Silva, N.R.B. Raposo, In vitro antifungal activity of hexahydropyrimidine derivatives against the causative agents of dermatomycosis, N. R. B, Sci. World J. (2017) 1–8, https://doi.org/10.1155/2017/1207061.

[7] V. Sharma, N. Chitranshi, A. K Agarwal, Significance and biological importance of pyrimidine in the microbial world, International Journal of Medicinal Chemistry (2014) 1–31, https://doi.org/10.1155/2014/202784.

[8] K.S. Jain, T.S. Chitre, P.B. Miniyar, M.K. Kathiravan, V.S. Bendre, V.S. Veer, S.R. Shahane, C.J. Shishoo, Biological and medicinal significance of pyrimidines, Curr. Sci. 90 (6) (2006) 793–803.

[9] S. Aayisha, T.S. Renuga Devi, S. Janani, S. Muthu, M. Raja, S. Sevvanthi, DFT, molecular docking and experimental FT-IR, FT-Raman, NMR inquisitions on "4-chloro-N-(4,5-dihydro-1H-imidazole-2-yl)-6-methoxy-2-methylpyrimidin-5-amine": alpha-2-imidazoline receptor agonist antihypertensive agent, J. Mol. Struct. 1186 (2019) 468–481, https://doi.org/10.1016/j.molstruc.2019.03.056.

[10] M. Sahu, N. Siddiqui, A review on biological importance of pyrimidines in the new era, Int. J. Pharm. Pharmaceut. Sci. 8 (5) (2016) 8–21.

[11] N. Burcu Arslan, Namık Özdemir, Osman Dayan, Necmi Dege, Koparır Metin, Pelin Koparır, Halit Muğlu, Direct and solvent-assisted thione–thiol tautomerism in 5-(thiophen-2-yl)-1, 3, 4-oxadiazole-2 (3H)-thione: experimental and molecular modeling study, Chem. Phys. 439 (2014) 1–11.

[12] Sevgi Kansız, Necmi Dege, Synthesis, Crystallographic structure, DFT calculations and Hirshfeld surface analysis of a fumarate bridged Co (II) coordination polymer, J. Mol. Struct. 1173 (2018) 42–51.

[13] S. Demir, S. Cakmak, N. Dege, H. Kutuk, M. Odabasoglu, R.A. Kepekci, A Novel 3-Acetoxy-2-Methyl-n-(4-Methoxyphenyl) Benzamide: molecular structural describe, antioxidant activity with use X-ray diffractions and DFT calculations, J. Mol. Struct. 1100 (2015) 582–591.

[14] S. Aayisha, T.S. Renuga Devi, S. Janani, S. Muthu, M. Raja, R. Hemamalini, Structural (PES), AIM, Spectroscopic profiling (FT-IR, FT-Raman, NMR and UV), HOMO-LUMO and Docking studies of 2,2-dimethyl-N-(2-pyridinyl)propanamide – a DFT approach, Chemical Data Collections 24 (2019) 100287, https://doi.org/10.1016/j.cdc.2019.100287.

[15] Walid Guerrab, Ill-Min Chung, Sevgi Kansiz, Joel T. Mague, Necmi Dege, Jamal Taoufik, Rachid Salghi, Ismat H. Ali, Mohammad I. Khan, Hassane Lgaz, Youssef Ramli, Synthesis, structural and molecular characterization of 2,2-diphenyl-2H,3H,5H,6H,7H-imidazo[2,1-b][1,3]thiazin-3-one, J. Mol. Struct. 1197 (2019) 369–376.

[16] Arulraj Ramalingam, Sevgi Kansız, Necmi Dege, Sivakumar Sambandam, Synthesis, crystal structure, DFT calculations and hirshfeld surface analysis of 3-chloro-2, 6-bis (4-chlorophenyl)-3-methylpiperidin-4-one, J. Chem. Crystallogr. 51 (2021) 273–287.

[17] Y. Sert, F. Ucun, G.A. El-Hiti, K. Smith, A.S. Hegazy, Spectroscopic investigations and DFT calculations on 3-(Diacetylamino)-2-ethyl-3H-quinazolin-4-one, Journal of Spectroscopy (2016) 1–15, https://doi.org/10.1155/2016/5396439.

[18] S. Bennia, R. Milad, S. Messaoudi, M. de Person, F. Moussa, M. Abderrabba, D. Merlet, Density Functional Theory based study on structural, vibrational and NMR properties of cis - trans fulleropyrrolidine mono-adducts, PLoS One 13 (11) (2018) e0207635, https://doi.org/10.1371/journal.pone.0207635.

[19] Tian Lu, Feiwu Chen, Multiwfn: A multifunctional wavefunction analyzer 33 (5) (2012) 580–592.

[20] A. Bajpai, V. Baboo, A. Dwivedi, Structural, electronic, and vibrational properties of isoniazid and its derivative N-Cyclopentylidenepyridine-4-carbohydrazide: a quantum chemical study, Journal of Theoretical Chemistry (2014) 1–15, https://doi.org/10.1155/2014/894175.

[21] D. Shoba, S. Periandi, S. Boomadevi, S. Ramalingam, E. Fereyduni, FT-IR, FT-Raman, UV, NMR spectra, molecular structure, ESP, NBO and HOMO–LUMO investigation of 2-methylpyridine 1-oxide: a combined experimental and DFT study, Spectrochim. Acta A 118 (2014) 438–447, https://doi.org/10.1016/j.saa.2013.09.023.

[22] A.K. Pandey, D.V. Shukla, V. Singh, V. Narayan, Structural, IR spectra NBO, TDDFT, AIM calculation, biological activity and docking property of [1,2,4]-triazolo [3,4-b][1,3,4] thiadiazole, Egyptian Journal of Basic and Applied Sciences 5 (4) (2018) 280–288, https://doi.org/10.1016/j.ejbas.2018.10.001.

[23] G. Jin-Sheng Gao, Y. Ying-Hui, L. Ying, H. Guang-Feng, Di-μ-chlorido-bis{[1,2-bis(pyridin-2-ylmethoxy)benzene-κ^4N,O,O′,N′]chloridocadmium, Acta Crystallophica Section E 67 (10) (2011) m1415. http://scripts.iucr.org/cgi-bin/paper?S1600536811037858.

[24] P. Panini, D. Chopra, Quantitative insights into energy contributions of intermolecular interactions in fluorine and trifluoromethyl substituted isomeric N-phenylacetamides and N-methylbenzamides, CrystEngComm 15 (2013) 3711–3733, https://doi.org/10.1039/c3ce40111a.

[25] G. Venkatesh, M. Govindaraju, P. Vennila, C. Kamal, Molecular structure, vibrational spectral assignments (FT-IR and FT-Raman), NMR, NBO, HOMO–LUMO and NLO properties of 2-nitroacetophenone based on DFT calculations, J. Theor. Comput. Chem. 15 (1) (2016) 1650007, https://doi.org/10.1142/s0219633616500073.

[26] A. Thamarai, R. Vadamalar, M. Raja, S. Muthu, B. Narayana, P. Ramesh, S. Aayisha, Molecular structure conformational analyses, solvent-electronic studies through theoretical studies and biological profiling of (2E)-1-(3-bromo-2-thienyl)-3-(4-chlorophenyl)-prop-2-en-1-one, J. Mol. Struct. (2019) 127349, https://doi.org/10.1016/j.molstruc.2019.127349.
[27] D. Durga devi, S. Manivarman, S. Subashchandrabose, Synthesis, molecular characterization of pyrimidine derivative: a combined experimental and theoretical investigation, Karbala International Journal of Modern Science 3 (2017) 18–28.
[28] V. Vetrivelan, Spectra, electronic properties, biological activities and molecular docking investigation on sulphonamide derivative compound: an experimental and computational anpproach, Journal of nanoscience and technology 4 (2) (2018) 348–352, https://doi.org/10.30799/jnst.sp203.18040203.
[29] J.M. Ramosa, C.A. Tellez Soto, Fourier transform infrared spectrum: vibrational assignments using density functional theory and natural bond orbital analysis of the bis(guanidoacetate)nickel(II) complex, Sci. Asia 37 (2011) 247–255, https://doi.org/10.2306/scienceasia1513-1874.2011.37.247.
[30] Trocia N. Clasp, Scott W. Reeve, Hideya Koizumi, Vibrational band assignment of 2-ethyl-1-hexanol, J. Theor. Comput. Chem. 16 (3) (2017) 1750023.
[31] M. Minteguiaga, E. Dellacassa, M.A. Iramain, C.A.N. Catalan, S.A. Brandan, The influence of acetate group on C2 is evidenced through NPA and MK charges FT-IR, FT-Raman, UV-Vis, NMR and structural studies of carqejyl actetate, a distinctive component of the essential oil from Baccharis trimera (less.) DC. (Asteraceae), J. Mol. Struct. 1177 (2019) 499–510, https://doi.org/10.1016/j.molstruc.2018.10.010.
[32] M. Ali, A. Mansha, S. Asim, M. Zahid, M. Usman, N. Ali, DFT study for the spectroscopic and structural analysis of p-dimethylaminoazobenzene, Journal of Spectroscopy (2018) 1–15, https://doi.org/10.1155/2018/9365153.
[33] S. Murugavel, V. Vetrivelan, D. Kannan, M. Bakthadoss, Synthesis, crystal structure analysis, spectral investigations, DFT computations, Biological activities and molecular docking of methyl(2E)-2-{[N-(2-formylphenyl)(4-methylbenzene) sulfonamido]methyl}-3-(4-fluorophenyl)prop-2-enoate, a potential bioactive agent, J. Mol. Struct. 1108 (2016) 50–167.
[34] J. Kausteklis, V. Aleksa, M.A. Iramain, S.A. Brandan, DFT and vibrational spectroscopy study of 1-butyl-3-methylimidazolium trifluromethanesulfonate ionic liquid, J. Mol. Struct. 1175 (2019) 663–676, https://doi.org/10.1016/j.molstruc.2018.08.014.
[35] G. Socrates, Infrared and Raman Characteristic Group Frequencies –-Tables and, third ed., Wiley, New York, 2001.
[36] V.R. Dani, Organic Spectroscopy, vol. 139, Tata-McGraw Hill Publishing Company, New Delhi, 1995.
[37] V. Vetrivelan, Spectra, Electronic structure, Biological activities and Molecular docking investigation on methyl (2E)-2-{[N-(2-formylphenyl)-4-methyl benzene sulfonamido] methyl}-3-(naphthalen-1-yl) prop-2-enoate: an experimental and computational approach, Mater. Today: Proc. 8 (1) (2019) 402–411, https://doi.org/10.1016/j.matpr.2019.02.129.
[38] J.P. Nascimento, J.R.A. Silva, J. Lameira, C.N. Alves, Metal-dependent inhibition of HIV-1 integrase by 5CITEP inhibitor: a theoretical QM/MM approach, Chem. Phys. Lett. 583 (2013) 175–179.
[39] S. Moro, M. Bacilieri, C. Ferrari, G. Spalluto, Autocorrelation of molecular electrostatic potential surface properties combined with partial leastsquares analysis as alternative attractive tool to generate ligand based 3D-QSARs, Curr. Drug Discov. Technol. 2 (2005) 13–21.
[40] V. Rajmohan, S. Deepa, S. Asha, S.V. Priya, Abir Sagaama, M. Raja, Synthesis, solvation effects, spectroscopic, chemical reactivity, topological analysis and biological evaluation of 4-chloro-N-(2, 6-dichlorobenzylidene) benzohydrazide, J. Mol. Liq. 390 (2023) 122955.
[41] D. Shoba, S. Periandi, S. Boomadevi, S. Ramalingam, E. Fereyduni, FT-IR, FT-Raman, UV, NMR spectra, molecular structure, ESP, NBO and HOMO–LUMO investigation of 2-methylpyridine 1-oxide: a combined experimental and DFT study, Spectrochim. Acta 118 (2019) 438–447, https://doi.org/10.1016/j.saa.2013.09.023.
[42] R. Rajasekar, T.S. Renuga Devi, S. Janani, M. Raja, Sunil Kumar, P. Ramesh, S. Muthu, Saleem Javed, Molecular structure, physicochemical properties, impact of solvents ionization potential, electron occupancy, inhibition constant, and stabilization energy investigations of 4-acetamido benzoic acid, Chemical Physics Impact 7 (2023) 100328.
[43] O.I. Osman, DFT study of the structure, reactivity, natural bond orbital and hyperpolarizability of thiazole azo dyes, Int. J. Mol. Sci. 18 (2) (2017) 239, https://doi.org/10.3390/ijms18020239.
[44] Z. Demircioğlu, C. Albayrak Kaştaş, O. Büyükgüngör, The spectroscopic (FT-IR, UV–vis), Fukui function, NLO, NBO, NPA and tautomerism effect analysis of (E)-2-[(2-hydroxy-6-methoxybenzylidene)amino]benzonitrile, Spectrochim. Acta 139 (2015) 539–548, https://doi.org/10.1016/j.saa.2014.11.078.
[45] J. Numbonui Ghogomu, N. Kennet Nkungli, A DFT study of some structural and spectral properties of 4-methoxyacetophenone thiosemicarbazone and its complexes with some transition metal chlorides: potent antimicrobial agents, Advances in Chemistry 2016 (2016) 1–15, https://doi.org/10.1155/2016/9683630.
[46] Mouna Medimagh, Cherifa Ben Mleh, I.S.S.A.O.U.I. Noureddine, Murugesan Raja, Aleksandr S. Kazachenko, M. Omar, Al-Dossary, Thierry Roisnel , Naveen Kumar and Houda Marouani, Bonding and noncovalent interactions effects in 2,6-dimethylpiperazine-1,4-diium oxalate oxalic acid: DFT calculation, topological analysis, NMR and molecular docking studies, Z. Phys. Chem. (2023), https://doi.org/10.1515/zpch-2023-0354.
[47] R.A. Costa, E.S. A Junior, J. de A. Bezerra, J.M. Mar, E.S. Lima, M.L.B. Pinheiro, K.M.T. Oliveira, Theoretical investigation of the structural, spectroscopic, electronic, and pharmacological properties of 4-nerolidylcathecol, an important bioactive molecule, J. Chem. (2019) 1–14, https://doi.org/10.1155/2019/9627404.
[48] P. Chakkaravarthy, V. Vetrivelan, S. Syed Shafi, S. Muthu, Spectroscopic (FT-IR & FT-Raman), Fukui function and molecular docking analysis of 6-amino-7,9-dihydropurine-8-thione by DFT approach, Bulg. Chem. Commun. 52 (4) (2020) 440–447.
[49] R. Buvaneswari, M. Simon Jeya Sunder Raj, K. Sudha, T. Aravind, P. Chakkaravarthy, M. Raja, Comprehensive analysis of (E)-3-(4-chlorophenyl)-1-(4-methoxyphenyl)prop-2-en-1-one (4CP4MPO): synthesis, Spectroscopic, salvation electronic properties, electron-hole transition, topological, Hirshfeld surface and molecular docking analysis, Chemical Physics Impact 8 (2024) 100452.